Research Square

Preprints are preliminary reports that have not undergone peer review.
They should not be considered conclusive, used to inform clinical practice,
or referenced by the media as validated information.

Recurrent flooding amid declining rainfall and increasing drought in the Baghmati–Adhwara Basin, India

Manu Raj Sharma

fakeersharma@gmail.com

Lalit Narayan Mithila University

Surbhi Kumari

Lalit Narayan Mithila University

Research Article

Keywords: Baghmati-Adhwara River Basin, Drought severity, Flood dynamics, Rainfall variability, Evapotranspiration, Water stress

Posted Date: November 26th, 2026

DOI: https://doi.org/10.21203/rs.3.rs-11659720/v1

License: This work is licensed under a Creative Commons Attribution 4.0 International License.
Read Full License

Additional Declarations: No competing interests reported.

Recurrent flooding amid declining rainfall and increasing drought in the Baghmati–Adhwara Basin, India

Manu Raj Sharma[1] and Surbhi Kumari [2]

[1] Assistant Professor, University Department of Geography, Remote Sensing Lab, Advanced Research Centre, LN Mithila University, Darbhanga

[2] Research Scholar, University Department of Geography, LN Mithila University, Darbhanga

Corresponding author: fakeersharma@gmail.com

1. Abstract

Droughts and floods are recurrent hydroclimatic hazards intensified by climate change and threaten agricultural livelihoods, environmental sustainability, and water security. The Baghmati-Adhwara River Basin (BARB) in North Bihar is particularly vulnerable to these extremes. This study examines flood patterns, drought severity, rainfall variability, and future precipitation trends using an integrated remote sensing, climatological, and statistical approach. Flood dynamics during 2017–2025 were assessed using pre- and post-flood Sentinel-1 Synthetic Aperture Radar (SAR) imagery, while drought conditions were evaluated through the Standardised Precipitation Index (SPI), Rainfall Anomaly Index (RAI), and MODIS-derived actual and potential evapotranspiration (ET and PET). Long-term rainfall variability (1901–2024) was analysed using the Modified Mann–Kendall test, and future rainfall trends were projected using XGBoost. Results identified 2017 as the most severe flood year, followed by 2020 and 2025, while 2023 experienced comparatively milder flooding. SPI indicated increasing drought frequency and persistent

moderate drought conditions, particularly after 2000. RAI revealed predominantly negative rainfall anomalies during 2010–2024, especially in Darbhanga, Madhubani, and Sitamarhi. Annual PET (1900–2700 mm) substantially exceeded ET (400–700 mm), indicating considerable atmospheric moisture demand and water stress. Long-term rainfall trends declined across all districts, with the steepest decreases in Madhubani (−2.5 mm yr^{-1}) and Darbhanga (−2.4 mm yr^{-1}). XGBoost projections indicate continued rainfall decline, particularly in these districts. These findings highlight increasing hydroclimatic vulnerability and the need for integrated drought–flood monitoring and climate-resilient water management.

Keywords: Baghmati-Adhwara River Basin; Drought severity; Flood dynamics; Rainfall variability; Evapotranspiration; Water stress

2. Introduction

The sharp edge of climate change is the escalating intensity and frequency of extreme weather, which presents a diverse array of evolving hazards to societies worldwide[1] . Climate change intensifies water scarcity by altering precipitation patterns, increasing extreme weather events, and raising temperatures, all of which cumulatively strain current water supplies[2]. Hydroclimatic extremes such as droughts and floods pose considerable and escalating challenges for urban and suburban areas worldwide. Over 50% of the world's population currently lives in urban areas, and by mid-century, that share is expected to rise to about 68%. This puts concentrated populations, vital infrastructure, and water systems at risk as environmental conditions change rapidly[3]. The total area of metropolitan areas worldwide that are susceptible to both drought and flooding is expected to increase by over 250% by 2030 relative to 2000[4]. Water scarcity is expected to affect almost half of the world's 482 largest cities by 2050.

Furthermore, without suitable mitigation and adaptation measures, 52% of the world's population and 45% of its GDP will be at risk of severe water scarcity by 2050[5]. The Climate Risk Index 2026 highlights India's high vulnerability to extreme weather, ranking it 9th globally over the past three decades (1995–2024), while in 2024 it ranked 15th overall for climate impact and 3rd for total affected population, behind Bangladesh and the Philippines [6]. In recent decades, climate-driven variability in hydro-meteorological factors alongside growing water demand has exacerbated mild-to-severe droughts worldwide, causing significant declines in soil moisture, groundwater storage, and streamflow[7]. At the same time, warmer air temperatures increase convective processes and atmospheric moisture capacity, increasing the frequency and severity of extreme rainfall events and urban flooding[8]. This has attracted considerable attention from the public and the scientific community in studies of hydroclimatic extremes. Floods occur when excessive precipitation, runoff, storm surges, or infrastructure breaches exceed the carrying capacity of natural and artificial drainage systems, leading to widespread inundation[9]. The WHO lists three types of floods: coastal, flash, and river. Due to a variety of socioeconomic and geographic factors,27 out of the 36 states and union territories in India are vulnerable to natural disasters[10]. A prolonged dry spell or a slow-onset phenomenon caused by insufficient precipitation is termed a drought[11]. It is regarded as one of the costliest disasters, imposing a greater burden on people and the economy than any other type of natural disaster. Drought is an irregular climatic feature that occurs across all regimes, with varying severity, duration, and extent[12]. It is mainly classified as meteorological, agricultural, and hydrological drought [13]. Using precipitation as an input parameter, researchers identify droughts through various indices. Meteorological droughts are detected with the Standardized Precipitation Index (SPI), Rainfall Anomaly Index (RAI), Effective Drought Index

(EDI), and Drought Area Index (DAI). Agricultural droughts are assessed using remote sensing and soil moisture-based indices such as the Enhanced Vegetation Index (EVI), Normalized Difference Vegetation Index (NDVI), Evaporative Stress Index (ESI), Soil Moisture Anomaly (SMA), Soil Moisture Deficit Index (SMDI), and Evapotranspiration Deficit Index (ETDI). Hydrological droughts are identified with indices like the Palmer Hydrological Drought Index, Standardized Streamflow Index, and the Streamflow Drought Index[14]. Large parts of the Earth are vulnerable to drought, which brings long-term social, economic, and environmental effects on regional demography[15]. It directly affects the environment, water, energy, social security, agriculture, tourism, the economy, ecosystems, and fundamental human welfare, often resulting in death and displacement.

Severe droughts have been observed across various climate zones worldwide over the last 10 years, causing significant social and economic impacts[13]. Extreme droughts affect regions differently, with wealthy nations experiencing less growth than underdeveloped countries. In 2021, California experienced drought conditions, resulting in substantial economic losses, especially in agriculture[16]. In 2022, one-third of Europe experienced its worst droughts, disrupting the economy by over EUR 40 billion and, combined with a hot summer, causing severe crop losses[13]. The Rhine River in Germany recorded its lowest levels, reducing capacity by 25-35% in 2022. After three years of drought, over 23 million people in the Horn of Africa faced severe hunger[17]. Long-lasting droughts occurred in South America, Asia, Africa, and North America from August 2023 to July 2024[18]. Droughts are increasing in South Asia, affecting crops, groundwater, livestock, and hydropower, leading to social and economic losses[19]. In the Asian monsoon region, droughts are linked to changes in rainfall patterns and water management[20]. Studies show that seasonal rainfall and temperature drive drought

severity in China's Yellow River Basin[21]. Drought patterns in Bangladesh are shifting, with the central region becoming more vulnerable. In Iran, precipitation largely explains drought variation over time[22].

Drought risk is increasing in India due to greater variability in the southwest monsoon and associated uncertainties. India has witnessed an overall rise in drought frequency since the 1960s, with notable rises during the 1980s, 2000s, and 2010s, with three major drought events per decade[23]. The percentage of land experiencing drought in central, northeast and west central India increased between 1950 and 2010, and the Representative Concentration Pathway (RCP) 8.5 scenario predicts that by 2095, the percentage of land under "above moderate drought" in India will rise to seventy per cent[24]. Droughts affect large regions in India, where densely populated regions like the Indo-Gangetic plains, coastal South India and central India have witnessed increased socio-economic vulnerability and food insecurity in recent decades[25]. Approximately one-fourth of India's population living in areas with depleted groundwater resources was affected by the drought from 2015 to 2018. Over the past decade, northern India has experienced an increase in the frequency of meteorological droughts at shorter timescales[26].

Rainfall variability is a fundamental driver of meteorological drought because changes in the amount, timing, duration, and seasonal distribution of precipitation directly influence water availability[27]. Drought may result not only from reduced annual or seasonal rainfall but also from prolonged dry spells and uneven rainfall distribution[28]. This is particularly important in monsoon-dependent regions, where rainfall is concentrated within a few months, and interannual variability can substantially affect soil moisture, groundwater recharge, surface-water availability, and agricultural water supply[29]. Multi-timescale indices such as SPI therefore help distinguish short-term precipitation

deficits affecting soil moisture from persistent deficits with broader hydrological implications[30] [31].

The Ganga-Brahmaputra basin is highly vulnerable to climate change and experiences both flood and drought conditions. The high-intensity rainfall in the Ganga-Brahmaputra basin's upstream regions (Nepal, Arunachal Pradesh, and Nagaland) is the primary cause of riverine floods in the basin's downstream regions. The Ganga-Brahmaputra basin experienced flooding in 2020 that inundated up to 19.48% (77,493.1 km2), negatively affecting both agricultural (23.68–28.47% of farmland area) and built-up regions (5.66–9.15% of built-up area). As a result, millions of people were affected by the floods, with Bihar suffering the most.[32] Meteorological drought intensity has increased in Indian River Basins, especially the Barak, Mahanadi, Indus, South Tapi, Ganga, and Brahmaputra[33]. The most intense drought conditions are found in the southwest Ganga Basin. Kaushik et al. studied dry spells in the Ganga-Brahmaputra basin from 1991 to 2020 and reported long, episodic droughts[34]. Most Indian river basins are more affected by hydrological and soil-moisture droughts than other basins. Singh et al. identified severe droughts in the Betwa and Kshipra basins using SPI, SRI (Standardized Runoff Index), and SPEI (Standardized Precipitation Evapotranspiration Index)[35]. Dwivedi et al. analyzed drought events in the Ken River Basin, noting droughts in 2007, 2015, and 2017 with SPI and RAI[36]. Singh et al. found the southern Harohar-Punpun Basin susceptible to prolonged dry spells using RAI and SPI[37]. Singh et al. used seven indices to identify drought in the Betwa Basin, finding mostly normal to moderate conditions, with SPI being the most effective indicator for drought management[38].

Rainfall variability alone, however, does not fully explain hydroclimatic water stress. Actual evapotranspiration (AET/ET) represents water actually transferred from the land surface and vegetation to the atmosphere, whereas potential evapotranspiration (PET)

represents atmospheric evaporative demand[39]. Under adequate moisture availability, rainfall can support higher ET, whereas under water-limited conditions ET may decline despite continued atmospheric demand represented by PET[40]. Consequently, the interaction among rainfall, ET, and PET provides complementary information on water availability and moisture stress. Combining these variables with SPI and RAI can therefore extend drought assessment beyond precipitation deficits to the broader condition of hydroclimatic water stress[41][42].

Bihar, a densely populated state in eastern India, is highly vulnerable to hydro-meteorological disasters. Every monsoon, numerous rivers originating in the Himalayas drain its catchments, making North Bihar one of the most fertile and populated regions in the Gangetic plains and also one of India's most flood-vulnerable regions [43]. The North Bihar plains receive adequate rainfall but experience drought spells in which annual rainfall declines by twenty-five per cent. The state is experiencing a decline in annual rainfall, affecting water availability[28]. Rainfall patterns are erratic, especially in the northeast and east, with the maximum annual rainfall dropping from 2769 to 2453 mm after 1982[44]. Studies using SPI identify mild-to-moderate droughts across Bihar, and even during the monsoons, crops remain vulnerable to water scarcity due to unpredictable rainfall[45]. A study investigated the 2021 flooding event in central Bihar utilising Sentinel-1 SAR data and identified two major flood surges: the initial on July 21, which predominantly affected Samastipur and Khagaria with considerable flooding adjacent to the Kosi River, and the subsequent on August 14, when Bhagalpur and Munger faced intense inundation, especially along the Ganges River[46]. Using Sentinel-1 SAR data, Bhatt et al. examined floods in the Gandak River Basin from 2017 to 2024 and found that over eight years, flood frequency peaked in 2020 (5.92%), followed by 2017 (5.86%), with 2017 experiencing the greatest loss [47]. SAR data and Digital

Elevation Model (DEM) have been used effectively to delineate flood extent and depth in the Kosi River basin in North Bihar[48,49]. According to a study, 39% of the Kosi River basin lies in high- to very-high-susceptibility flood zones, exposing 2.69 million people to flood risk [50]. Tuladhar et al. observed that most rain gauge stations near the Baghmati River catchment received less rainfall[51], with drought conditions intensifying over two decades[52]. The Baghmati–Adhwara River Basin (BARB) in North Bihar's Indo-Gangetic Plain is a key agricultural area with a dense population, heavily reliant on rainfall and prone to floods and droughts. The right bank of the Baghmati River frequently floods because of its shape, terrain, and high water flow, which reactivates small channels and spills water into low areas [53]. Recent studies from Madhubani, a major part of the North Bihar region, have highlighted important linkages between rainfall variability, drought, wetland conditions, and evapotranspiration. Sharma et al. reported substantial rainfall variability, declining rainfall, and emerging dry spells in Madhubani, with implications for wetland hydrology and ecosystem sustainability[54]. Similarly, Sharma and Das (2026) demonstrated relationships among rainfall, actual and potential evapotranspiration, water deficit (WD), wetness, and vegetation productivity during 2002–2024[55]. These studies provide important regional evidence that rainfall variability and evapotranspiration dynamics are closely associated with water availability and hydroclimatic stress. Although previous research has explored drought in Bihar and surrounding basins using indices such as SPI and RAI, understanding of the long-term, multi-timescale, and integrated hydroclimatic characteristics of drought in the BARB remains limited. Specifically, the combined analysis of precipitation deficits, rainfall variability, evapotranspiration, and atmospheric water demand represented by potential evapotranspiration has received limited attention. Moreover, existing studies have largely focused on recent periods and specific wetland

landscapes, leaving a gap in basin-wide, long-term assessment. The connection between historical drought variability and future rainfall projections at the basin and district levels also remains underexplored, limiting understanding of how changing rainfall patterns and evaporative demand may influence future water scarcity in the BARB.

This study aims to fill these gaps by providing a comprehensive assessment of drought dynamics and hydroclimatic variability in the BARB from 1901 to 2024. It will analyse drought characteristics using multi-timescale SPI and RAI, evaluate long-term rainfall trends with the Modified Mann–Kendall test and Sen's slope, examine actual and potential evapotranspiration to understand water availability and atmospheric water demand, and explore relationships among rainfall, ET, and PET to identify hydroclimatic stress. The study also employs the XGBoost algorithm to project future rainfall variability. By integrating these elements, the research aims to deepen understanding of drought-related hydroclimatic stress and support better drought monitoring, climate adaptation, and sustainable water management in the BARB.

3. Study Area

The Baghmati Adhwara River Basin (BARB) is part of the Himalayan river system, which drains southward through Bihar (India) and Nepal. The Baghmati River rises in Nepal's Shivpuri Mountain and drains a basin of approximately 8848 square kilometres. The river is 589 km long; 394 km lie in Bihar, and the remaining 195 km flow in Nepal. The study area extends between 25º41'54.9"N and 26º52'36.8" N latitude and 85º37'28.20"E and 86º20'38.936"E longitude (Fig. 1). The Kamla-Balan River Basin forms the eastern boundary of the research area, the Budhi Gandak Basin forms the western boundary, and the Himalayas form the northern boundary. The Baghmati's tributaries form an intricate network: some merge into the river, while others diverge from the main flow as the river braids. Tributaries such as Lakhandei, Darbhanga

Baghmati, and Old Kamla join its left bank, while Lal Bakiya and Hasanpur Baghmati form its right-bank tributaries.

In Bihar, the river passes through Sitamarhi, Sheohar, East Champaran, Muzaffarpur, Darbhanga, Samastipur, Khagaria, and Begusarai. After travelling downstream through these districts and before the confluence with the river Kosi, it is characterized by a single-channel meandering river system. According to Koppen's climate classification, the Baghmati Adhwara River Basin falls in the subtropical monsoon (Cwa) region, where monsoonal rainfall plays a significant role. For the present analysis, the annual climatic cycle is divided into four seasons: winter (January-February), pre-monsoon/summer (March-May), southwest monsoon (June-September), and post-monsoon/autumn (October-December). The southwest monsoon is the principal rainy season and contributes the dominant share of annual precipitation, whereas the pre-monsoon period is generally characterized by increasing temperatures and comparatively lower rainfall. Winter is predominantly dry and cooler, while October–December represents the post-monsoon transition from the rainy season to winter. The basin's average annual precipitation is 1190 mm (IMD, 2025). Heavy rainfall from the south-west monsoon contributes to the large sediment load and frequent overbank flooding in the Baghmati River basin. In addition to being a hydrologically dynamic doab zone, the Baghmati River basin faces the dual challenges of drought and flooding.

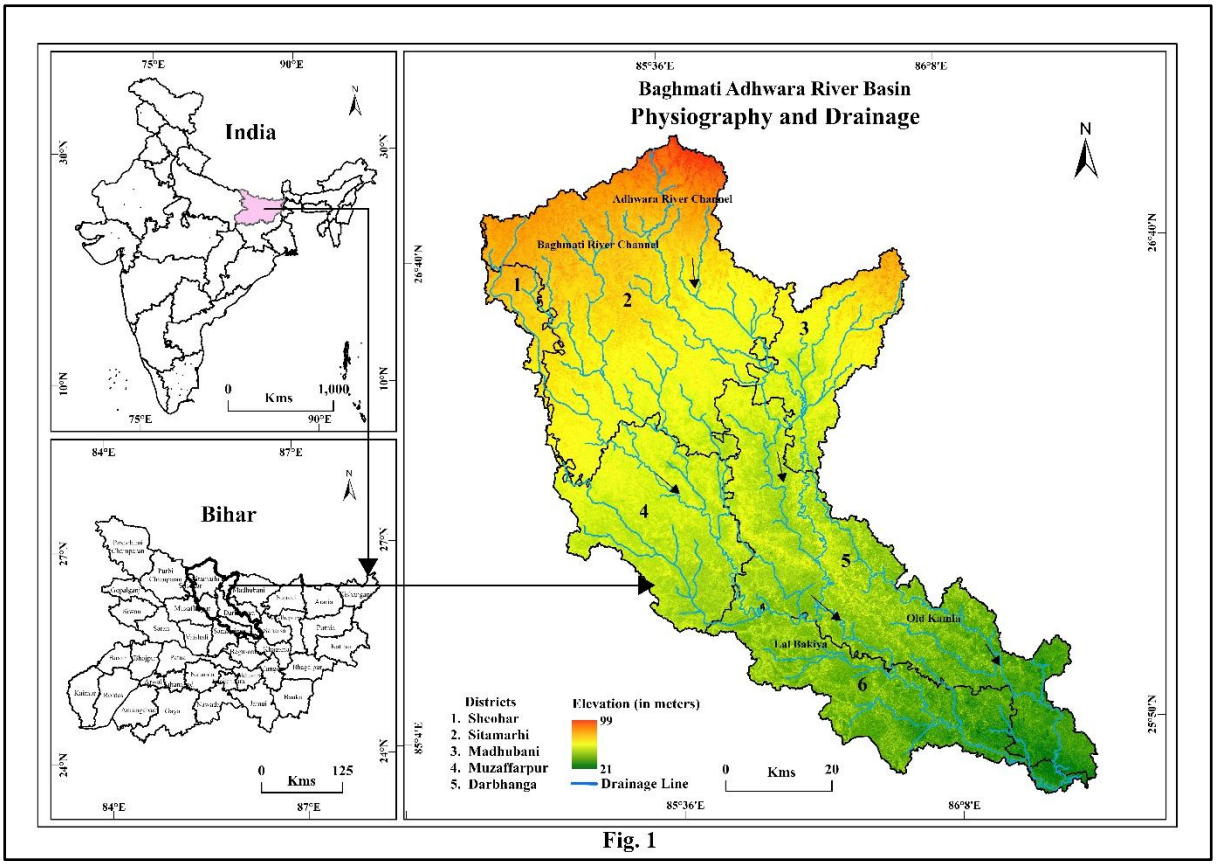

Fig. 1

4. Database and Methodology

This study integrates meteorological, topographical, and remotely sensed datasets to investigate the spatio-temporal characteristics of rainfall and associated hydrological processes in the BARB (Fig. 2). It uses district-level rainfall data from the India Meteorological Department (IMD), Patna, covering 1901-2024. The Digital Elevation Model (DEM) of the BARB was procured from the Shuttle Radar Topography Mission (SRTM) of the United States Geological Survey (USGS) at a 30-meter spatial resolution to understand the physiography, drainage, and delineation of the study area. The DEM was generated only to delineate the study area and represent topography and drainage. Evapotranspiration (ET) plays a crucial role in moisture cycling and water movement through evaporation and transpiration, making it an essential part of the hydrological cycle [56]. In this research, satellite-derived ET and potential evapotranspiration (PET) data were sourced from the Terra MODIS MOD16A2GF product covering 2002–2023.

The MOD16A2GF, with a 500 m spatial resolution and an 8-day composite interval, was employed to analyse the spatial, seasonal, and temporal patterns of evapotranspiration in the Bagmati–Adhwara River Basin. The ET and PET values were converted to millimetres per 8-day period using the recommended scale factor of 0.1.

Latent heat flux (LE) was estimated from evapotranspiration (ET) using the relationship

$$LE = \lambda E,$$

where, LE represents latent heat flux (W m $^{-2}$), E is the evapotranspiration rate (kg m $^{-2}$ s $^{-1}$), and λ is the latent heat of vaporization of water (J kg $^{-1}$). The MODIS ET values, originally expressed in millimetres per 8-day period, were converted to an equivalent water flux prior to estimating LE. LE was included to quantify the energy associated with evapotranspiration and to complement the water-flux perspective provided by ET. The resulting LE estimates were used to examine the relationship between precipitation, evapotranspiration, and surface energy exchange in the BARB.

The MODIS-derived ET/PET record is shorter than the rainfall record used in this study. This difference in temporal coverage was purposefully maintained because each dataset serves a different analytical function. The long-term rainfall dataset (1901–2024) was used to analyse historical rainfall variability, trends, droughts, wetness conditions, and anomalies. In contrast, the MODIS record (2002–2023) focused on recent spatially detailed evapotranspiration dynamics. The datasets were not combined into a single continuous time series over 1901–2024. When comparing rainfall with ET/PET, the analysis was limited to their overlapping period (2002–2023) to ensure consistency over time.

Flood inundation was mapped using Sentinel-1 SAR imagery. Sentinel-1 operates at C-band microwave frequencies and remains impervious to cloud cover, making it especially effective for flood mapping in this region, where monsoonal cloud cover

significantly limits the utility of optical imaging during peak flooding events [50]. Sentinel-1 GRD imagery was acquired from the COPERNICUS/S1_GRD collection covering floods from 2017 to 2025. The VH (cross-polarisation) channel was chosen as the primary detection band because it shows more distinct bimodal differentiation between water and land backscatter values in vegetated agricultural floodplains.

4.1 Data Quality Control and Pre-processing:

Before analysis, all datasets underwent quality-control procedures to ensure completeness, consistency, and suitability for the respective analyses. The IMD rainfall series (1901–2024) was examined for missing, duplicate, and inconsistent observations, and identified gaps were addressed using the specified interpolation procedure based on available long-term observations. Missing observations in the IMD rainfall series were addressed using mean imputation, replacing missing values with the mean of the available rainfall observations. This procedure was applied to identified gaps to maintain continuity of the 1901-2024 rainfall series required for annual and seasonal rainfall analysis, SPI and RAI calculation, and future rainfall projection. The Sentinel-1 SAR images utilised for flood mapping were pre-processed in ESA SNAP following a standardized workflow to ensure consistency and accuracy in flood detection. This preprocessing sequence included radiometric calibration, speckle filtering, terrain correction, and conversion of backscatter values to decibels (dB). Initially, SAR images were downloaded and imported into SNAP. Radiometric calibration converted raw digital numbers into physically meaningful backscatter coefficients (σ^0), enabling comparisons across time. A speckle filter was then applied to reduce granular noise and enhance the visibility of flooded areas. Terrain correction used a DEM to correct geometric distortions and accurately align the images with geographic and GIS data. The

calibrated images were converted from linear scale to dB, making flood signatures easier to interpret because water surfaces typically exhibit low backscatter values. Only VH polarization data were retained and exported as GeoTIFF files for further analysis in ArcGIS Pro. The MODIS MOD16A2GF ET/PET dataset was assessed for spatial and temporal completeness and invalid or missing pixel values, and the prescribed scale factor of 0.1 was consistently applied. The SRTM DEM was checked for complete spatial coverage and consistency before basin delineation and drainage extraction. These quality-control and pre-processing procedures were completed before subsequent statistical and spatial analyses. The following sections describe the theoretical background, computational procedures, and applications of these methods.

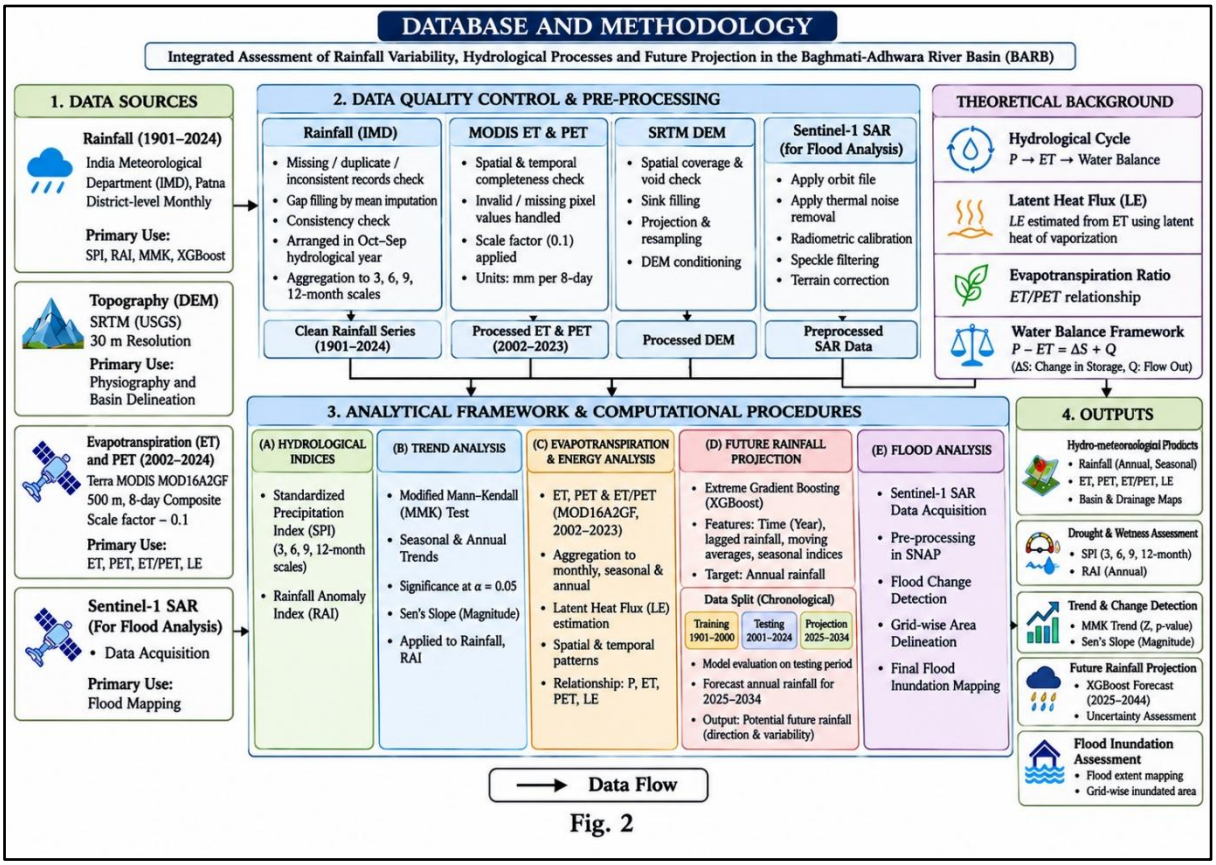

Fig. 2

4.2 Standardized Precipitation Index (SPI)

The Standardized Precipitation Index (SPI) is a frequently used indicator across the world for detecting and describing meteorological droughts. It compares observed total precipitation quantities over an accumulation period of interest (e.g., 1, 3, 12, 48 months) with the monthly district-level rainfall records for 1901–2024 obtained from the India Meteorological Department (IMD), Patna, to determine precipitation anomalies at a specific site[57]. SPI values range from -2 to +2, with negative values denoting drought-like conditions and positive values denoting wet conditions[58]. SPI was calculated using DrinC software following [59]. The monthly rainfall series was continuous, with the Indian hydrological year (June–May) used for annual analysis. SPI-12 reflects 12-month accumulated precipitation and indicates prolonged surplus or deficit, making it ideal for drought detection. The SPI has a mean around zero; positive values are wetter, negative are drier. Values typically range from −2 to +2, but can be outside this range. Classification thresholds indicate moderate dryness (−1.0 to −1.49), severe dryness (−1.5 to −1.99), extreme dryness (≤−2.0), and extreme wetness (≥2.0).

The SPI can be expressed as:

$$SPI = \Phi - 1[F(P)]$$

Where P is the precipitation amount for the selected time scale, F(P) is the cumulative probability of precipitation obtained from the fitted gamma distribution, and Φ^{-1} is the inverse standard normal distribution function[27]. SPI is appropriate for meteorological, precipitation-based drought assessment, while its limitation of excluding temperature/evaporative demand is addressed through your complementary SPEI and PET/ET analyses.

4.3 Rainfall Anomaly Index (RAI)

The Rainfall Anomaly Index (RAI) measures and monitors variations in rainfall patterns. RAI values range from -3 to +3. RAI values greater than 0 indicate above-normal

rainfall, and values less than 0 indicate below-normal rainfall. In this study, we estimated RAI values for each district. It is estimated using the formula:

$RAI = 3\left(\frac{P-\overline{P}}{\overline{P}_{10}-\overline{P}}\right)$ for positive anomalies and $RAI = -3\left(\frac{P-\overline{P}}{\overline{P}-\overline{P}_{10}}\right)$ for negative anomalies

Where, P is the observed rainfall, $\overline{P}$ is the long-term mean rainfall, and $\overline{P}_{10}$ is the mean of the ten highest rainfall values[60]. The RAI was included to provide a direct assessment of the magnitude and direction of rainfall anomalies relative to the long-term rainfall record, whereas SPI standardizes precipitation anomalies over specific accumulation periods to characterize drought severity and duration.

4.4 Modified Mann-Kendall Test

The modified Mann-Kendall (MMK) method is a refined version of the Mann-Kendall test, suitable for autocorrelated data due to its modified variance. The Modified Mann-Kendall test has been used to identify seasonal and annual rainfall trends. It is particularly advantageous for hydro-meteorological time series because rainfall data may exhibit temporal dependence and may not follow a normal distribution. Unlike parametric trend tests, it does not require the data to satisfy assumptions of normality and is relatively robust to outliers and non-linear trends.

Mann-Kendall Test Statistic (S)

$$S = \sum_{k=1}^{n-1} \sum_{j=k+1}^{n} \operatorname{sgn}(x_j - x_k)$$

where

$$\operatorname{sgn}(x_j - x_k) = \begin{cases} +1, & x_j - x_k > 0 \\ 0, & x_j - x_k = 0 \\ -1, & x_j - x_k < 0 \end{cases}$$

n= number of observations, and $x_j$and x_k are data values at times $j$and k.

Variance of S

For data with tied values:

$$Var(S) = \frac{n(n-1)(2n+5) - \sum_{p=1}^{g} t_p\,(t_p-1)(2t_p+5)}{18}$$

where:

1. g= number of tied groups
2. t_p= number of observations in the p-th tied group

Modified Variance (Hamed and Rao, 1998)

The MMK test adjusts the variance using an effective sample size (n^*):

$$Var^*(S) = Var(S) \times \frac{n}{n^*}$$

where

$$\frac{n}{n^*} = 1 + \frac{2}{n(n-1)(n-2)} \sum_{i=1}^{n-1} (n-i)(n-i-1)(n-i-2)\,\rho_s(i)$$

and:

1. n^*= effective sample size
2. $\rho_s(i)$= significant autocorrelation coefficient at lag i

Standardized Test Statistic (Z)

$$Z = \begin{cases} \dfrac{S-1}{\sqrt{Var^*(S)}}, & S > 0 \\ 0, & S = 0 \\ \dfrac{S+1}{\sqrt{Var^*(S)}}, & S < 0 \end{cases}$$

Interpretation

1. $|Z| > 1.96$: Significant trend at the 95% confidence level ($\alpha = 0.05$)
2. $|Z| > 2.576$: Significant trend at the 99% confidence level ($\alpha = 0.01$)

The Modified Mann–Kendall test was performed at a 5% significance level (α = 0.05).

4.5 Extreme Gradient Boosting (XGBoost)

XGBoost, or Extreme Gradient Boosting, is an ensemble learning algorithm that involves sequentially creating several trees, each of which attempts to reduce prior errors[61]. It was selected to investigate potential future rainfall dynamics because rainfall variability may involve non-linear, complex patterns that simple linear forecasting approaches may not adequately represent. It was therefore used to complement the statistical trend analysis and estimate potential future rainfall behaviour.

In XGBoost, each decision tree consists of a series of branching rules that divide the input data into smaller groups based on predictor values. The first tree produces an initial prediction, while subsequent trees are sequentially added to identify and reduce the errors (residuals) of the preceding trees. The final prediction combines the contributions of all trees. This sequential error-correction process enables XGBoost to capture non-linear relationships and complex variations in the rainfall series.

The annual rainfall data for 1901–2024 (124 years) were divided chronologically into a training period (1901–2000) and a testing period (2001–2024). The training dataset was used to develop the XGBoost model, while the testing dataset was used to evaluate its predictive performance using observations not included during model training. Random shuffling was avoided to preserve the chronological order of the time series. After model evaluation, the trained forecasting framework was used to estimate potential annual rainfall for 2025–2044. Thus, the modelling sequence was 1901–2000 (training) → 2001–2024 (testing and evaluation) → 2025–2044 (future projection). The resulting

projections were used to assess the potential direction and variability of future rainfall dynamics rather than to represent deterministic predictions of future climate conditions.

4.6 Flood Inundation Mapping

Flood inundation was mapped using Sentinel-1 SAR imagery processed in ESA SNAP. After pre-processing, the data were retained and exported as GeoTIFF files for further analysis in ArcGIS Pro. The SAR scenes were then merged and clipped to match the study area boundary. Flood areas were identified using change detection methods followed by ISO Cluster unsupervised classification into six classes. This classification was reclassified into two main categories: flooded and non-flooded areas. A grid-based sampling framework was overlaid on the flood maps, and the percentage of flooded area was calculated for each grid cell. These data formed the basis of a statistical flood database for temporal analysis and validation.

4.7 Flood-detection Accuracy Assessment

A confusion matrix approach was used to estimate the classification performance. The accuracy of Sentinel-1-derived flood inundation was assessed by comparing the Sentinel-1 flood maps for year 2021 and 2022 with the corresponding FMIS/RADARSAT flood maps. FMIS/RADARSAT was considered the reference dataset, while Sentinel-1 was treated as the classified dataset. Both datasets were harmonized to a common spatial reference, extent and grid before pixel-wise comparison. Flood and non-flood classes were cross-tabulated to generate a binary confusion matrix comprising true positive, false positive, false negative and true negative observations. Overall Accuracy, Producer's Accuracy, User's Accuracy, F1-score, Intersection over Union and Cohen's Kappa were subsequently calculated to quantify the agreement and flood-detection performance of

Sentinel-1. Separate accuracy assessments were conducted for 2021 and 2022 to examine date-specific consistency with the FMIS/RADARSAT reference inundation.

Each pixel was classified as:

1. True Positive (TP): Both datasets identify flood.
2. False Positive (FP): Sentinel-1 identifies flood, but FMIS/RADARSAT does not.
3. False Negative (FN): FMIS/RADARSAT identifies flood, but Sentinel-1 does not.
4. True Negative (TN): Both datasets identify non-flood.

A 2 × 2 confusion matrix was prepared for each date, and the following accuracy measures were calculated: Overall Accuracy, Producer's Accuracy, User's Accuracy, F1-score, IoU and Cohen's Kappa.

	FMIS/RADARSAT Flood	FMIS/RADARSAT Non-flood
Sentinel-1 Flood	TP	FP
Sentinel-1 Non-flood	FN	TN

The main equations are:

$$OA = \frac{TP + TN}{TP + TN + FP + FN} \times 100$$

$$PA = \frac{TP}{TP + FN} \times 100$$

$$UA = \frac{TP}{TP + FP} \times 100$$

$$F1 = \frac{2TP}{2TP + FP + FN}$$

$$IoU = \frac{TP}{TP + FP + FN}$$

Cohen's Kappa was used to measure the agreement between Sentinel-1 and FMIS/RADARSAT beyond chance.

5. Results

The BARB receives about 1180 mm of rain yearly, with over eighty per cent from the southwest monsoon, driven by systems originating over the Bay of Bengal. Post-monsoon depressions and cyclones also bring heavy rainfall, while winter rain comes from western disturbances. Changes in the amount, timing and persistence of rainfall can substantially influence agricultural water availability, soil moisture, wetlands and other water-dependent activities. The following sections examine long-term rainfall variability, precipitation anomalies, drought conditions, rainfall trends, and potential future changes across the basin.

5.1 Understanding Precipitation Deficit using Standardized Precipitation Index (SPI)

Quantifying SPI was used to quantify precipitation anomalies and identify the persistence of dry and wet conditions at 3-, 6-, 9-, and 12-month accumulation scales. Precipitation deficit at different time scales is a key feature of SPI. These time intervals (3, 6, 9, and 12 months) represent drought duration and its effects on water availability. SPI-3 shows an immediate impact on soil moisture and provides a seasonal estimate of precipitation, whereas SPI-6 and SPI-9 reflect short- and medium-term moisture conditions, and SPI-12 reflects persistent long-term precipitation deficits and surpluses. Prolonged negative SPI-12 conditions may reduce water availability and increase hydrological stress; however, SPI alone cannot infer direct impacts on streamflow and reservoir storage. SPI-based rainfall analysis indicates that the BARB is experiencing increasingly severe drought. The region has experienced severe and numerous mild droughts over the last two decades.

Based on SPI-3 analysis (Fig. 3), the study area exhibits recurrent short-term precipitation deficits. Persistent negative SPI-3 values indicate periods of below-normal precipitation that may increase moisture stress, particularly for rainfed agricultural activities and small surface-water bodies. This deficit has spiked in the last twenty years. Similarly, the SPI-6 (Fig. 4) and SPI-9 (Fig. 5) series indicate recurrent medium-term precipitation deficits across the districts, although their magnitude and persistence vary spatially. Several negative episodes extend across multiple months, suggesting periods of sustained moisture stress.

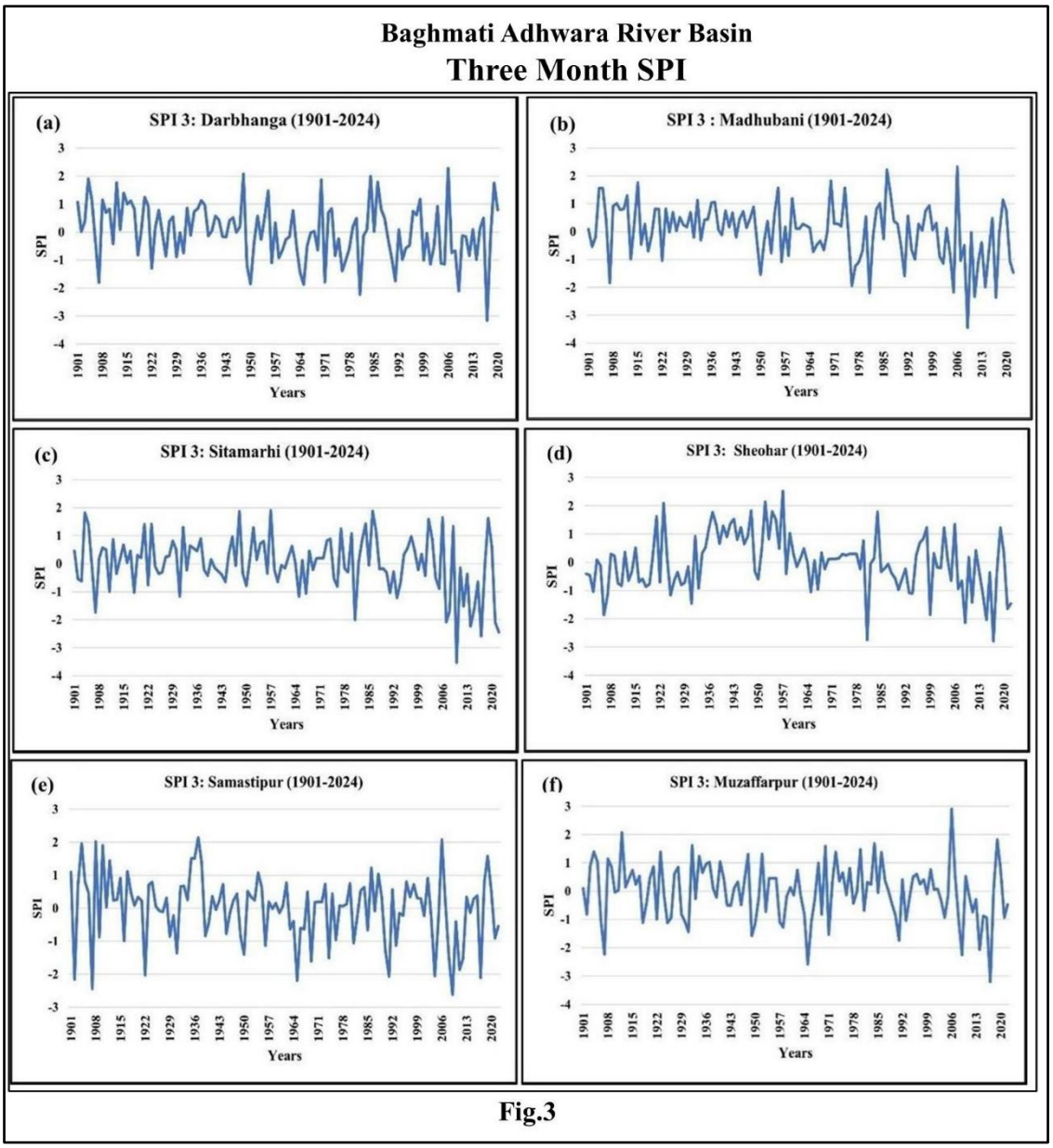

Fig.3

The SPI-12 results (Fig. 6) provide further evidence of prolonged precipitation variability and recurrent long-term dry conditions, particularly during the recent decades.

The SPI-12 series for six districts (Fig. 6a–f) offers a long-term view of precipitation variability from 1901–2024, showing significant interannual fluctuations with alternating wet and dry periods. The variability differs among districts, with several years showing very strong deficits or surpluses. Darbhanga (Fig. 6a) exhibits recurrent dry and wet episodes, with negative SPI-12 values during the 1930s, late 1980s-early 1990s, and especially during the 2000s and 2010s, indicating increasing long-term deficits. Madhubani (Fig. 6b) also

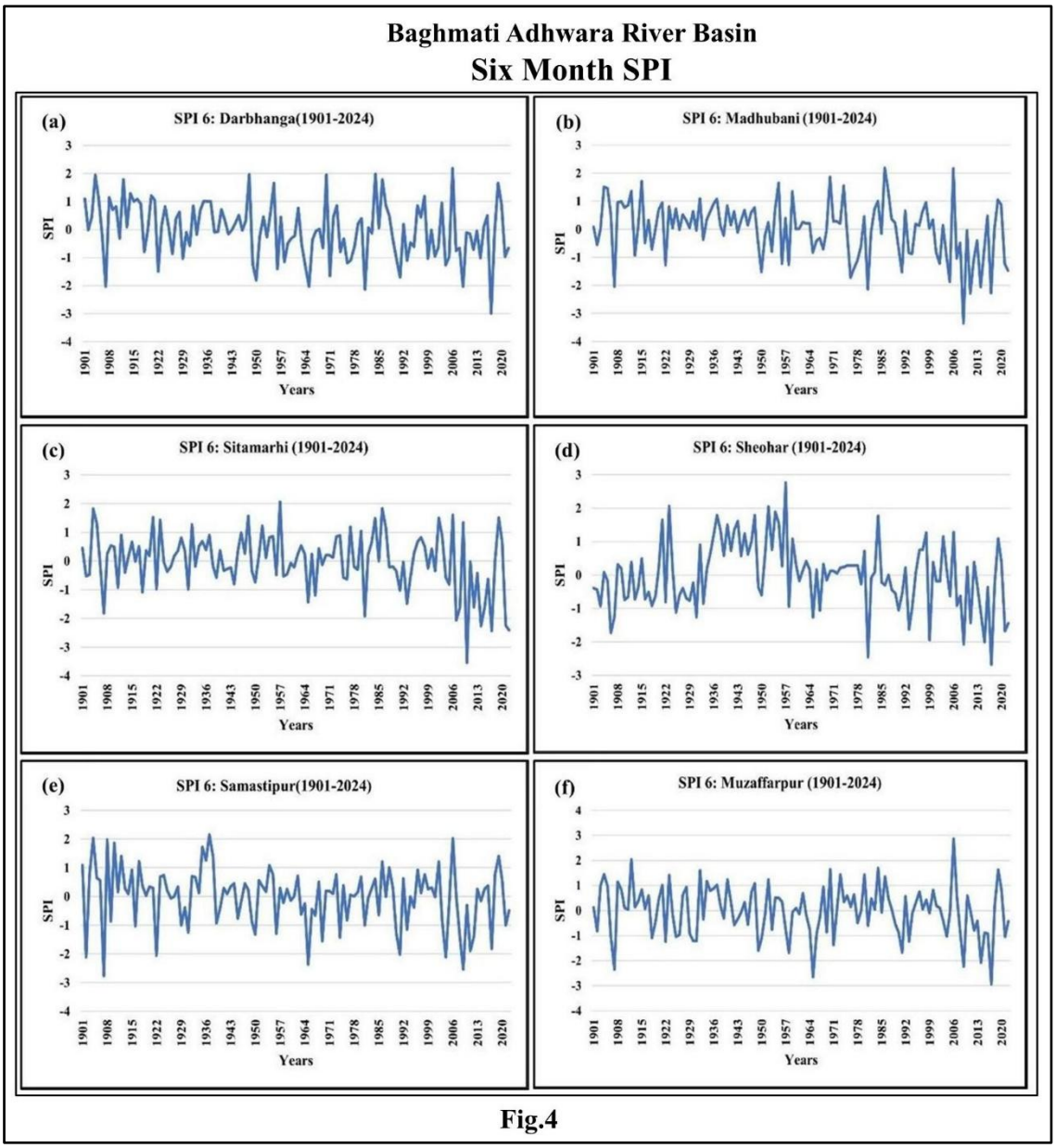

Fig.4

shows variability; early records fluctuate, but post-2000 periods have more negative values, especially in the late 2000s- 2010s, indicating recurring deficits amid some wet years. Sitamarhi (Fig. 6c) shows recurrent dry and wet episodes; negative values, especially below −2, become frequent in the 2000s-2010s, reflecting severe long-term dry conditions. Sheohar (Fig. 6d) shows a wet phase from the 1930s to 1950s, followed by increased variability in later decades, with significant dry spells in the 2000s-2010s, indicating a shift toward greater variability and recurrent droughts. Samastipur (Fig. 6e) displays notable fluctuations, with increasing negative SPI-12 years after 2000, indicating

long-term deficits

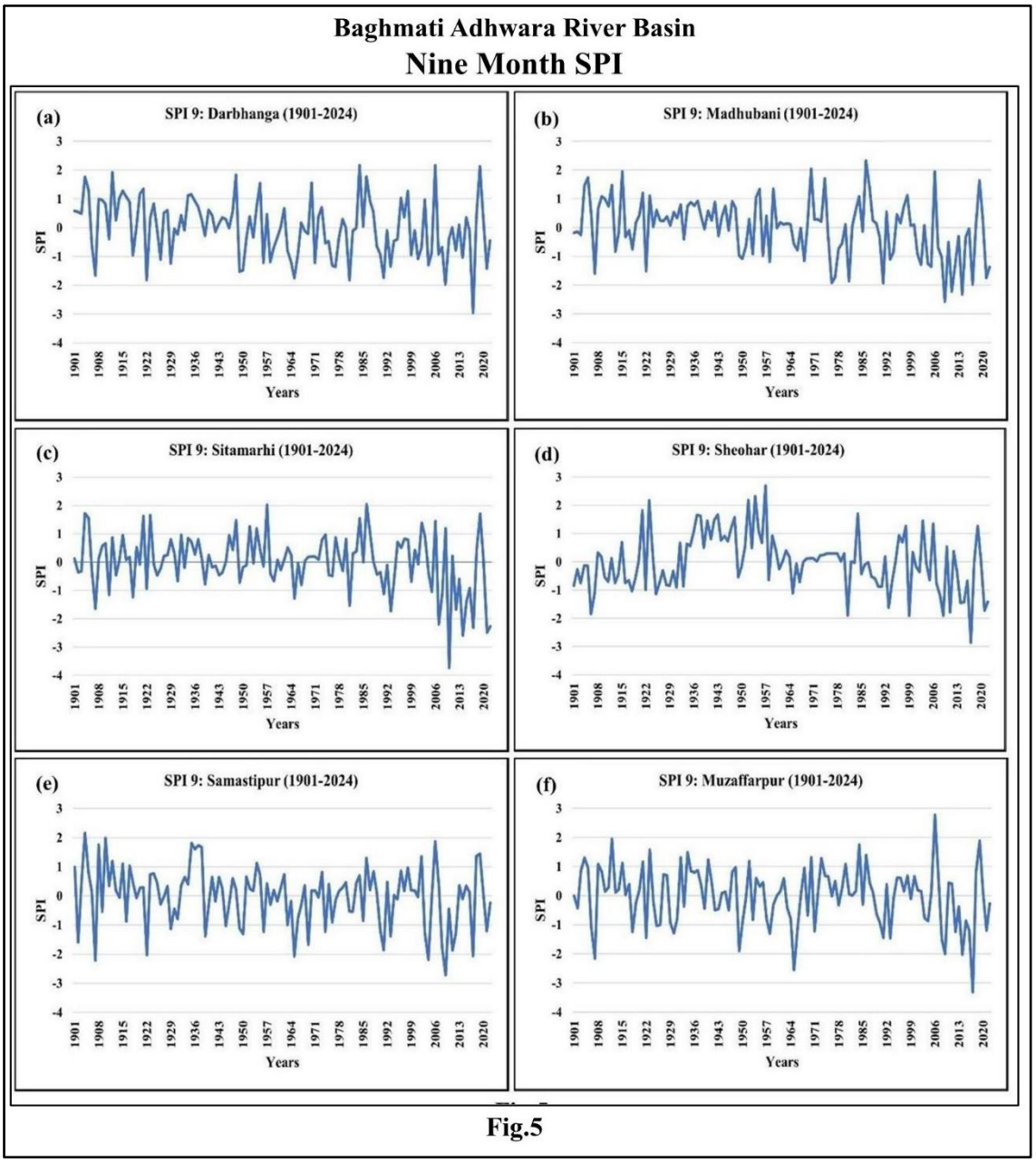

Fig.5

with some wet years. Muzaffarpur (Fig. 6f) shows alternating wet and dry periods, with stronger negative values after 2000, including extremely dry years, interrupted by wet years. Overall, the analysis reveals that long-term droughts have become more common across the basin, especially after 2000, with varying timing and intensity among districts. The basin now experiences more variable conditions with recurrent dry episodes, alongside positive extremes, indicating fluctuating precipitation patterns rather than uniform drying.

Overall, the SPI results reveal a spatially differentiated drought pattern across the BARB. The northern and northeastern districts, particularly Madhubani, Sitamarhi, and Sheohar, show a more persistent and pronounced shift toward negative SPI values in recent decades, with recurrent moderate-to-severe dry conditions evident across multiple time scales (SPI-3 to SPI-12). In contrast, the southern and central parts, represented by Darbhanga, Samastipur, and Muzaffarpur, exhibit greater alternation between wet and dry conditions, although recurrent negative SPI values and prolonged dry spells are also evident during the recent period. Thus, the recent intensification of drought is spatially widespread across the basin, but appears more persistent in its northern and northeastern sectors.

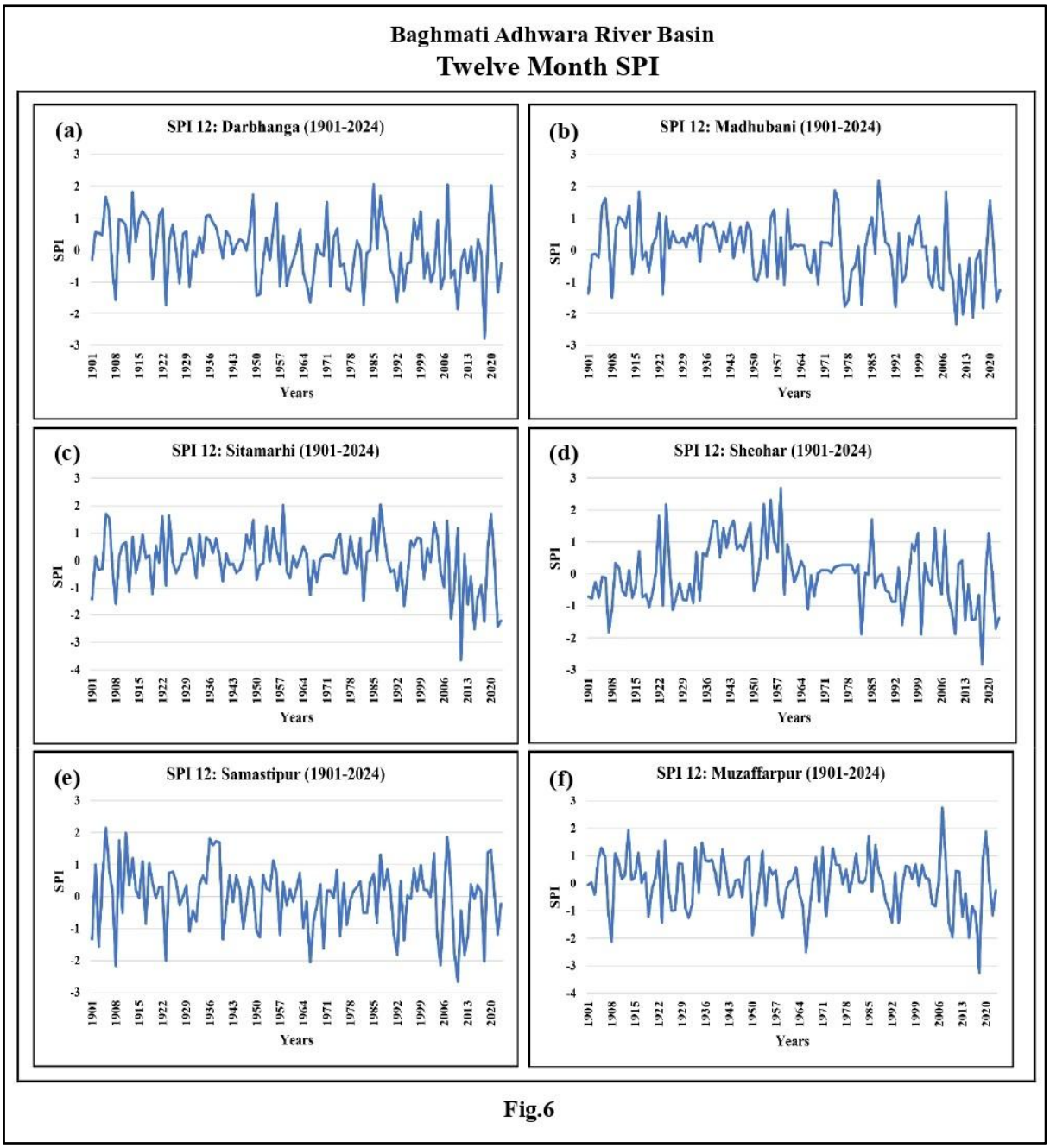

Fig.6

5.2 Evaluation of Annual Rainfall Variability using Rainfall Anomaly Index

The Rainfall Anomaly Index (RAI) was used to assess interannual variability and departures from normal annual rainfall across the Bagmati–Adhwara River Basin (BARB) during 1901-2024. Fig. 7 shows substantial year-to-year fluctuations, with alternating positive and negative rainfall anomalies across all six districts. The fitted linear regression lines indicate an overall decline in RAI across all districts from 1901-

2024, although the magnitude of the decline varies spatially. The strongest negative slopes are observed in Madhubani (−0.0027 year^{-1}), Darbhanga (−0.0018 year^{-1}), and Sitamarhi (−0.0020 year^{-1}), followed by Sheohar (−0.0015 year^{-1}) and Samastipur (−0.0014 year^{-1}), whereas Muzaffarpur exhibits the weakest declining slope (−0.0008 year^{-1}). The low R^2 values, however, indicate substantial interannual variability around these long-term linear tendencies.

The temporal distribution of anomalies also shows that negative RAI values are more frequent and persistent in recent decades, particularly after 2000, in several districts. This feature is especially evident in Darbhanga and Madhubani, where repeated negative anomalies occur during the 2000s and 2010s. Sitamarhi and Sheohar similarly show a concentration of negative anomalies in the latter part of the record, while Samastipur also shows several consecutive dry years in the recent period. Muzaffarpur shows smaller, less persistent negative anomalies, consistent with its weaker long-term declining slope. Thus, Fig. 7 suggests a spatially differentiated long-term drying tendency accompanied by greater recurrence of below-normal rainfall in recent decades.

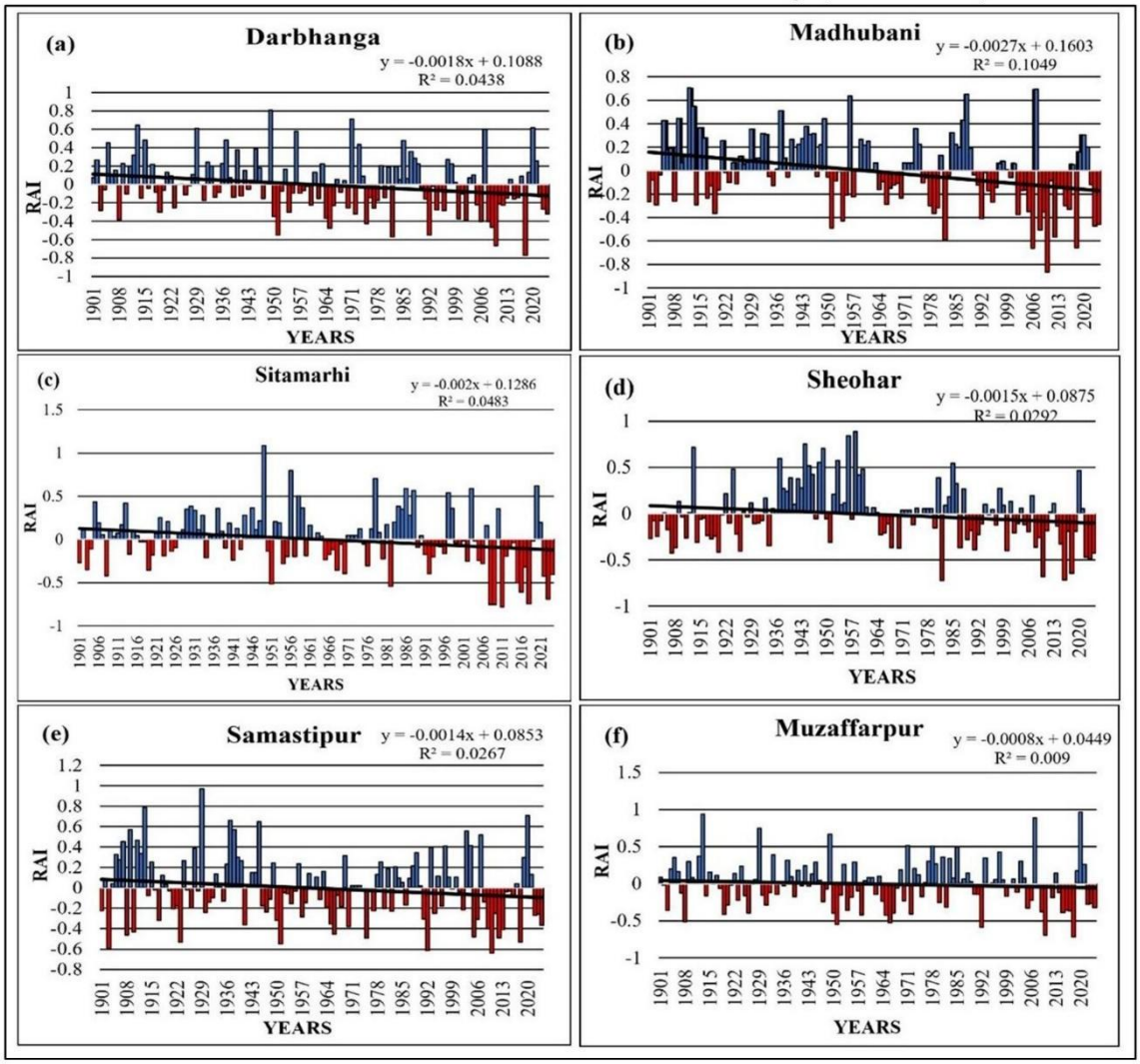

Fig.7

Recent years (2010-2024) have experienced a rise in negative rainfall anomalies across the BARB, notably in eastern districts like Sitamarhi, Madhubani, and Darbhanga. The RAI results largely align with the SPI findings, both showing a trend toward increasingly negative (dry) anomalies, especially after 2000. This pattern is particularly clear in Darbhanga, Madhubani, Sitamarhi, and Sheohar, highlighting a shared trend of growing precipitation deficits and drought occurrences over recent decades. Larger negative anomalies indicate drier conditions, leading to increased water scarcity, groundwater depletion, and reduced crop yields, especially for water-intensive crops like rice,

556 *makhana* (foxnut) and *singhada* (water chestnut). Commercial farming faces higher costs
557 and lower incomes, burdening farmers. Wetlands and aquaculture, vital for income in this
558 region, are also affected by less rainfall.

559 **5.3 Annual and Seasonal Rainfall Trends using Modified Mann-Kendall (MMK)**
560 **Test**

561 The Modified Mann-Kendall test is widely used to analyze trends in hydrological,
562 meteorological, and climatic data because of its insensitivity to outliers and its
563 independence from the normal probability distribution function (PDF) condition. In this
564 study, the MMK test was used to evaluate historical trends in annual and seasonal
565 rainfall. Table 1 lists the MMK test results. The Z_s score represents the rainfall trend
566 statistic for the study region from 1901 to 2024. The results showed a significant
567 decreasing rainfall trend across all districts of the Baghmati-Adhwara River, except
568 Sheohar. Table 1 also shows Sen's Slope, which indicates the rate of change in annual
569 rainfall across all districts from 1901 to 2024. The Sen's Slope value for all six districts,
570 viz. Darbhanga (2.4 mm), Madhubani (2.5 mm), Sitamarhi (1.7mm), Sheohar (1.1mm),
571 Samastipur (1.7mm), and Muzaffarpur (1.4 mm) showed a decreasing annual rainfall
572 rate. Among all districts, Madhubani and Darbhanga recorded the highest decline in
573 rainfall. This shows that Madhubani and Darbhanga, which are rich in wetlands, are
574 losing approximately one rainy day each year, threatening the areal distribution of
575 wetlands in these districts. Although Sheohar has the lowest Sen's Slope value (-1.19) in
576 the BARB, it also exhibits a non-significant decline in rainfall. The declining rainfall
577 trend across the region threatens the sustainability of water bodies and the region's water-
578 based economy, potentially affecting rural livelihoods. Seasonal analyses used rainfall
579 data for the winter, summer, monsoon, and post-monsoon seasons. Fig. 8a illustrates the
580 rainfall trend during winter. The districts of Sitamarhi in the north and Samastipur in the

581 south show a significant decrease in rainfall, whereas other districts show a decrease but
582 an insignificant trend.

583 **Table 1: Result of Modified Mann-Kendall Test (Annual)**

584

Districts	Z_s score	Sen Slope (Qs)	Interpretation
Darbhanga	**-3.76**	**-2.42**	***Significant decrease***
Madhubani	**-3.45**	**-2.58**	***Significant decrease***
Sitamarhi	**-2.29**	**-1.70**	***Significant decrease***
Sheohar	-0.67	-1.19	*Insignificant decrease*
Samastipur	**-2.29**	**-1.72**	***Significant decrease***
Muzaffarpur	**-2.07**	**-1.44**	***Significant decrease***

585 Summer season witnesses an insignificant decreasing rainfall trend in all the northern
586 districts of BARB, while an insignificant increasing rainfall trend can be seen in all the
587 southern districts of BARB (Fig. 8b). The result found out significant decreasing rainfall
588 trend in the entire BARB with Sheohar being an exception during the monsoon (Fig. 8c).
589 There is variability in BARB's rainfall trend during the post-monsoon season. All the
590 districts show a decreasing rainfall trend, with Sheohar and Madhubani showing a
591 significant decreasing trend, while the other 3 districts represent an insignificant
592 decreasing trend, with Samastipur being a notable exception (Fig. 8d). The annual
593 analysis of MMK test shows a significant decreasing rainfall trend in all districts of the
594 Baghmati-Adhwara River except Sheohar (Fig. 8e). It symbolises the decrease in
595 cyclonic rainfall in this study region. The analysis of annual and seasonal rainfall trends
596 from 1901 to 2024 in BARB reveals a decreasing trend across the entire region, with
597 minimal seasonal variation.

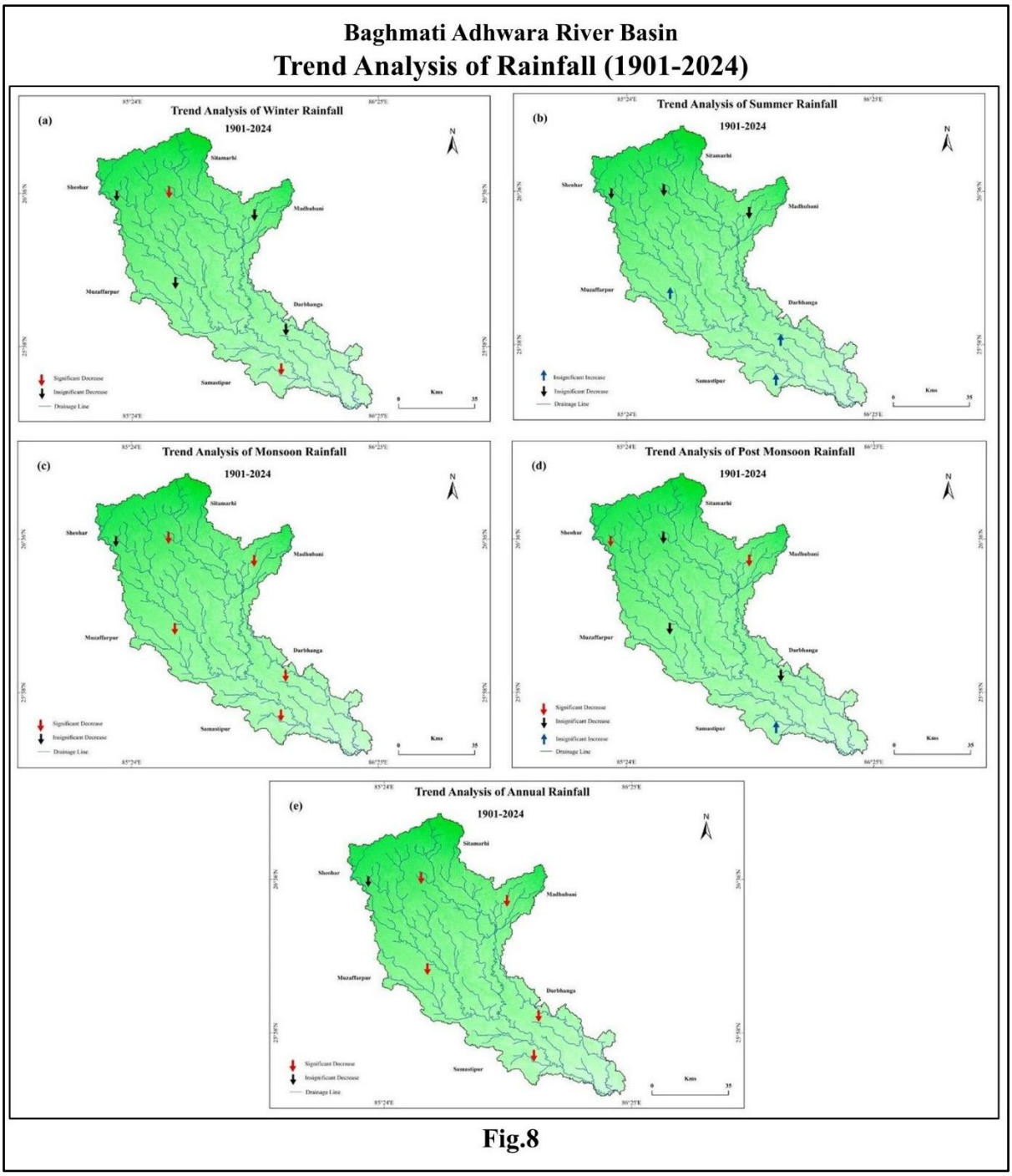

Fig.8

5.4 Projected Trends of Rainfall

The XGBoost model projects the trend of annual rainfall across the study region over the forthcoming decades (until 2044). The forecasts indicate generally lower rainfall conditions in several districts, accompanied by substantial interannual variability. Madhubani and Darbhanga will experience a significant reduction in rainfall relative to

other districts. Darbhanga will experience a decline in annual rainfall, with values ranging from 500 mm to 1300 mm (Fig. 9a). The projected values represent annual rainfall totals (mm) for each individual forecast year, rather than the amount of rainfall decline per year.

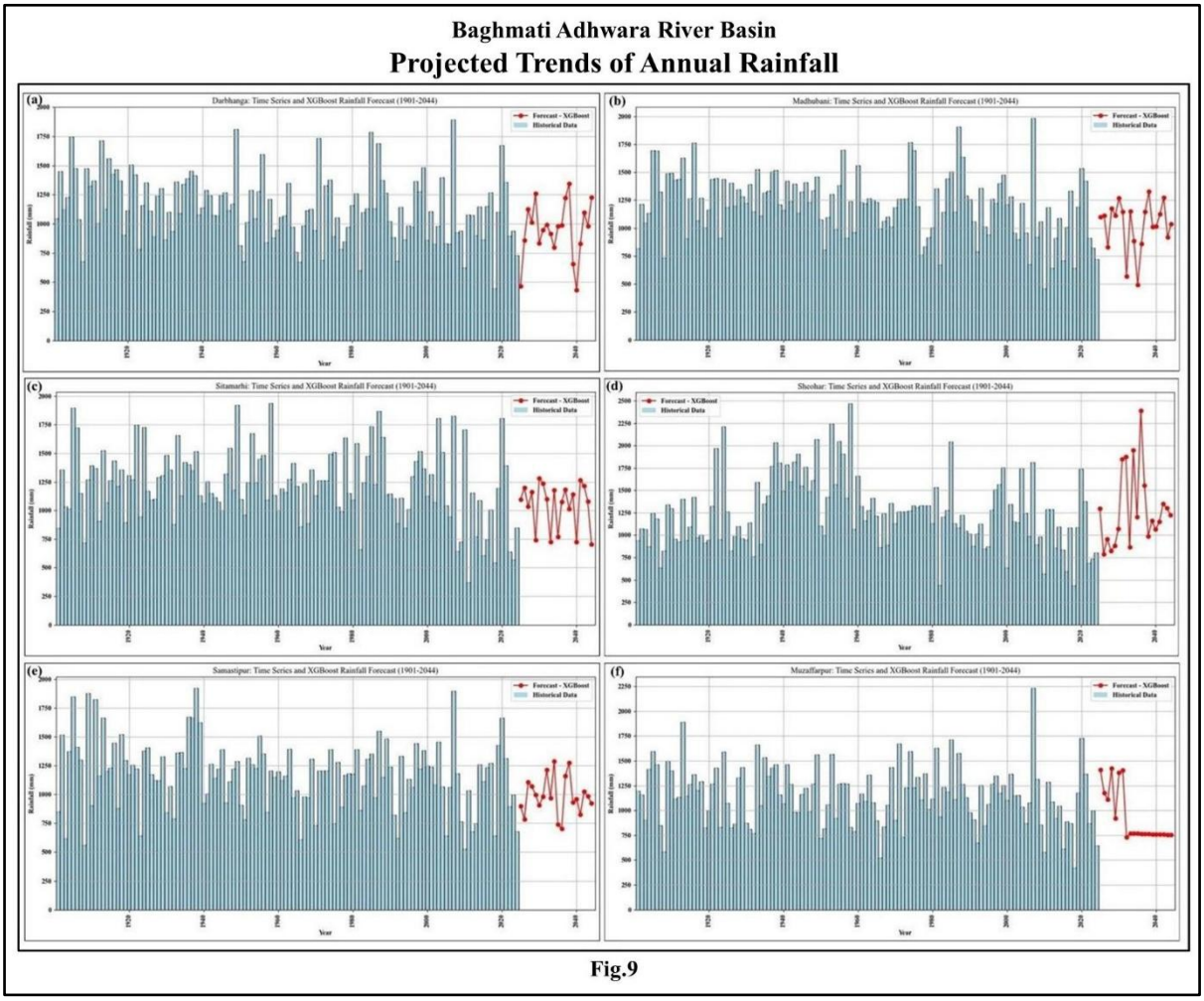

Fig.9

Similarly, Madhubani, where the average annual rainfall lies between 1200 and 1250 mm, future projections indicate a drop of 100-150 mm (Fig. 9b). Since both Madhubani and Darbhanga districts are rich in wetlands and rely heavily on water-based economic activities, this decline could severely impact livelihoods, agriculture, and wetland ecosystems. In Sitamarhi the average annual rainfall is expected to rise slightly over the next one to two years, followed by a steady decline, with values ranging between 750 mm and 1200 mm (Fig. 9c). Sheohar is projected to experience extreme fluctuations,

with average annual rainfall ranging from 800 mm to 2200 mm over the next two decades (Fig. 9d). Samastipur is projected to experience minimal fluctuations, with average annual rainfall ranging from 700 mm to 1300 mm over the next two decades (Fig. 9e). Muzaffarpur shows greater variability, with an initial decrease in rainfall, a brief increase, and a subsequent continuous decline (Fig. 9f).

The results indicate that the BARB will experience a decline in future rainfall, which may significantly affect the region's ET and PET. Reduced soil moisture and transpiration due to lower rainfall will lead to lower evapotranspiration, whereas higher temperatures and lower humidity will increase atmospheric moisture demand, resulting in higher PET.

This declining rainfall trend in the BARB is likely to significantly affect the streamflow of the Baghmati-Adhwara group. A decline in rainfall will reduce the river's water supply, leading to lower streamflow and potentially impairing the river’s ability to maintain its natural flow. With a notable reduction in rainfall in the coming years, the region may face an increased risk of meteorological drought. The projected decline in annual rainfall may increase the risk of reduced water availability, with potential implications for streamflow, groundwater recharge, agriculture, and wetland sustainability. Quantification of these impacts, however, requires independent hydrological and sector-specific modelling. Also, XGBoost projections do not explicitly represent future extreme rainfall events because this model was developed using annual rainfall totals; consequently, the projected series does not resolve short-duration, high-intensity precipitation events.

5.5 Annual Cycle of Evapotranspiration and Potential Evapotranspiration

Actual evapotranspiration (ET) and potential evapotranspiration (PET) offer complementary insights into water and energy exchanges between the land surface and

atmosphere. PET indicates the atmospheric evaporative demand when water supply is not a limiting factor, while ET measures the actual water transferred from the land via evaporation and plant transpiration. Comparing ET and PET helps evaluate how much surface-water availability and environmental conditions constrain evapotranspiration. From 2002 to 2023, monthly, seasonal, and yearly ET and PET data were estimated for the Bagmati Adhwara River Basin (BARB) using MODIS-based information. The findings reveal significant temporal and seasonal fluctuations in both.

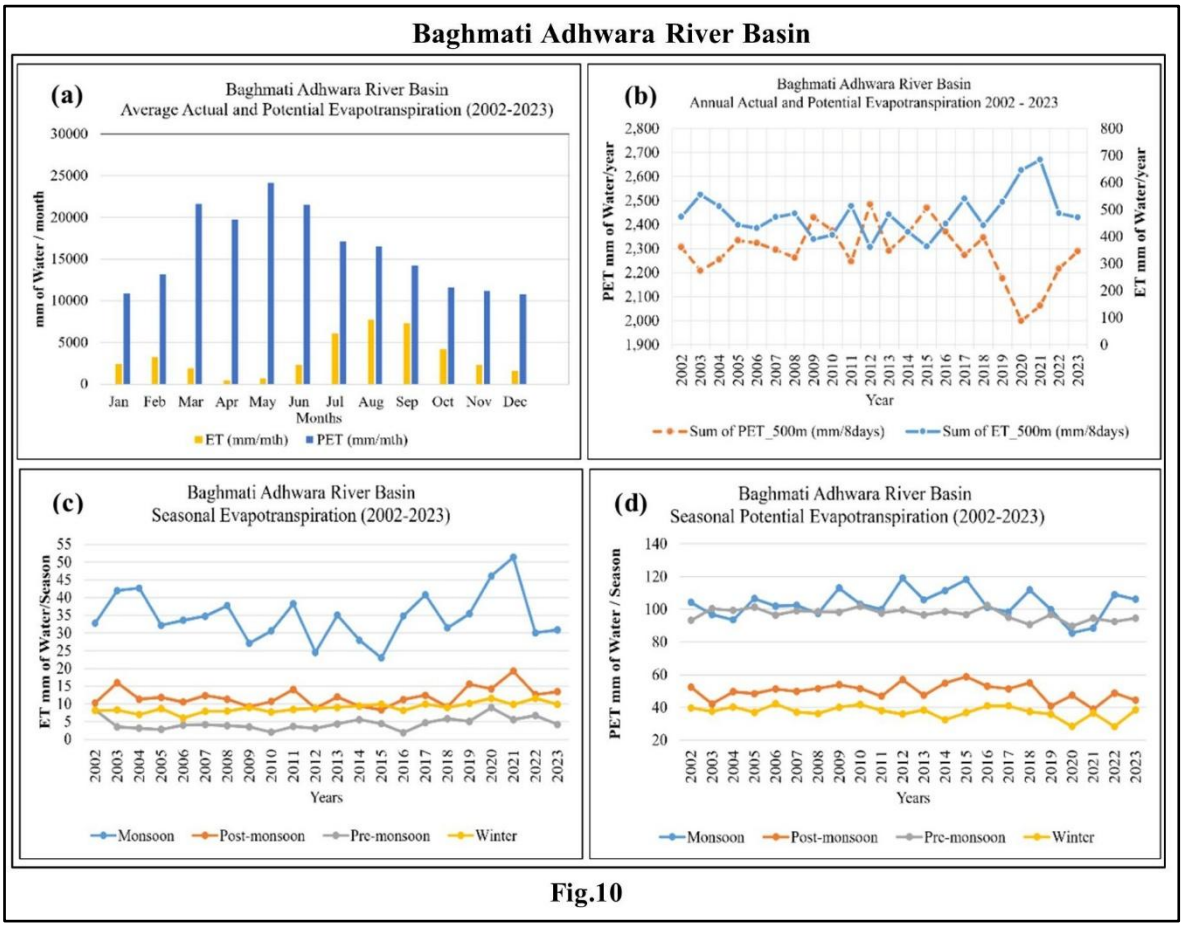

Fig.10

Fig. 10a presents the average monthly ET and PET for 2002–2023. PET is substantially higher than ET throughout the year, with the largest PET values occurring from spring through the monsoon and into early autumn. Seasonal variation in PET is primarily driven by changes in available energy, solar radiation, temperature, humidity, and other atmospheric controls on evaporative demand. ET, in contrast, depends on both

atmospheric demand and the availability of water at the land surface, as well as vegetation and soil conditions. Consequently, the difference between PET and ET indicates the extent to which actual evapotranspiration is constrained relative to atmospheric evaporative demand. The persistent ET-PET difference therefore suggests that actual evapotranspiration is frequently constrained by water availability and/or other land-surface controls; however, ET-PET differences alone should not be interpreted as direct evidence of below-average rainfall or drought.

Annual ET and PET from 2002 to 2023 are compared in Fig. 10b. PET remains considerably higher than ET throughout the study period, with annual PET generally ranging from approximately 1900 to 2700 mm, while annual ET is substantially lower, approximately 400-700 mm. The large separation between PET and ET indicates that the basin has a high atmospheric evaporative demand relative to the amount of water actually transferred through evapotranspiration. Year-to-year variability in ET is greater than in PET, particularly in the latter part of the study period. This variability may reflect changes in surface-water availability, vegetation conditions, soil moisture, and climatic factors. Although reduced rainfall can lower ET by reducing available soil and surface water, ET and PET alone cannot establish this relationship. Therefore, assess rainfall variability independently before attributing changes in ET specifically to a rainfall deficit.

The seasonal comparison further illustrates the contrast between atmospheric evaporative demand and actual evapotranspiration (Fig. 10c and 10d). During the monsoon season, PET ranges approximately from 85 to 120 mm per season, whereas ET ranges from approximately 23-51 mm per season. The relatively higher ET during the monsoon than in other seasons is consistent with more favourable evapotranspiration conditions, including greater atmospheric moisture and seasonal vegetation activity. Nevertheless, PET remains

higher than ET, indicating that actual evapotranspiration does not reach the potential atmospheric demand.

During the pre-monsoon season, PET is approximately 90-100 mm per season, whereas ET is much lower, approximately 1-11 mm per season. The large difference between PET and ET indicates strong moisture limitation and restricted water availability during the pre-monsoon period. This pattern is consistent with conditions in which atmospheric evaporative demand is high, but the water available for actual evaporation and transpiration is limited. However, low ET relative to PET does not, by itself, demonstrate below-average rainfall; such an inference requires independent rainfall-anomaly or precipitation data.

Winter and post-monsoon periods also generally show lower ET than PET. During these periods, reduced temperature and atmospheric energy, seasonal vegetation changes, and variations in surface-water availability can limit actual evapotranspiration. Therefore, the persistent seasonal difference between ET and PET indicates that actual evapotranspiration is often below atmospheric evaporative demand. This difference is particularly pronounced during the pre-monsoon period, suggesting a strong seasonal moisture constraint. Overall, the ET-PET comparison indicates that the BARB experiences substantial temporal and seasonal differences between atmospheric evaporative demand and actual water use. The results provide evidence of evaporative or moisture limitation, particularly during the pre-monsoon season.

5.6 Spatial Pattern of Flood Inundation

Flood inundation mapping for the Baghmati Adhwara River Basin was conducted using Sentinel-1 SAR data, ESA SNAP, and GIS techniques. Flood inundation was mapped for 2017, 2020, 2023, and 2025. A grid-oriented sampling structure was superimposed on the flood inundation maps and the proportion of flooded area was determined for each grid

unit. The results show moderate to severe flood inundation throughout the river basin in 2017 (Fig.11a). The most significant inundation is concentrated in the southeastern area (lower catchment), where Grid 1 experiences severe, persistent flooding that encroaches toward the lower Grid 2. The central region is also heavily affected, showing dense patches of inundation in Grid 5 that extend upward into Grid 6, along with significant dispersed flooding in Grid 4. In contrast, the northern boundary grids (Grids 8 and 9) and the eastern region (Grid 7) exhibit minimal flood extent during this year. The 2020 map (Fig.11b) reflects severe and widespread flood inundation across the river basin, with strong localised concentrations of floodwaters.

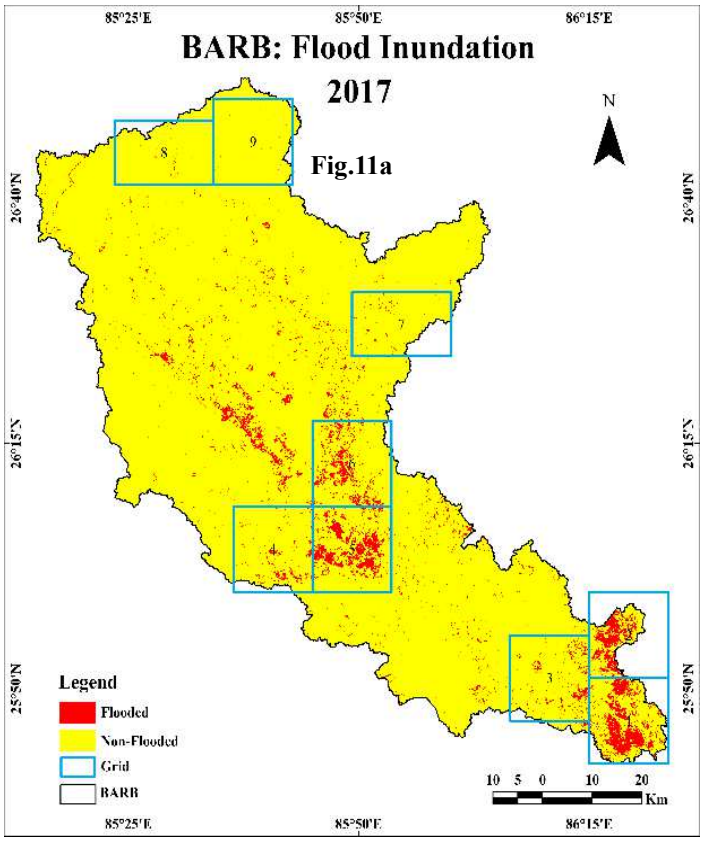

Fig.11a

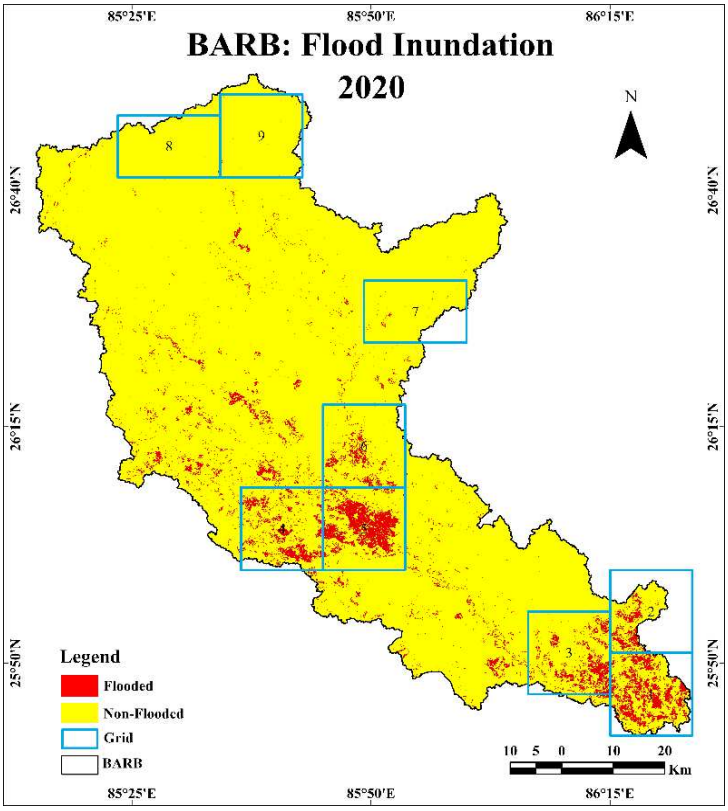

726

Fig.11b

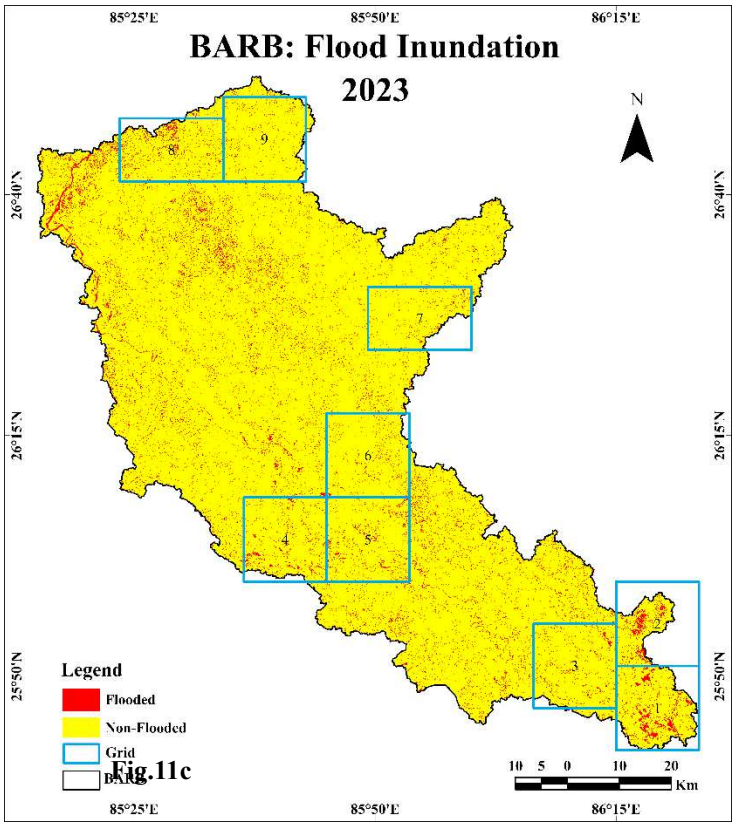

Fig.11c

727

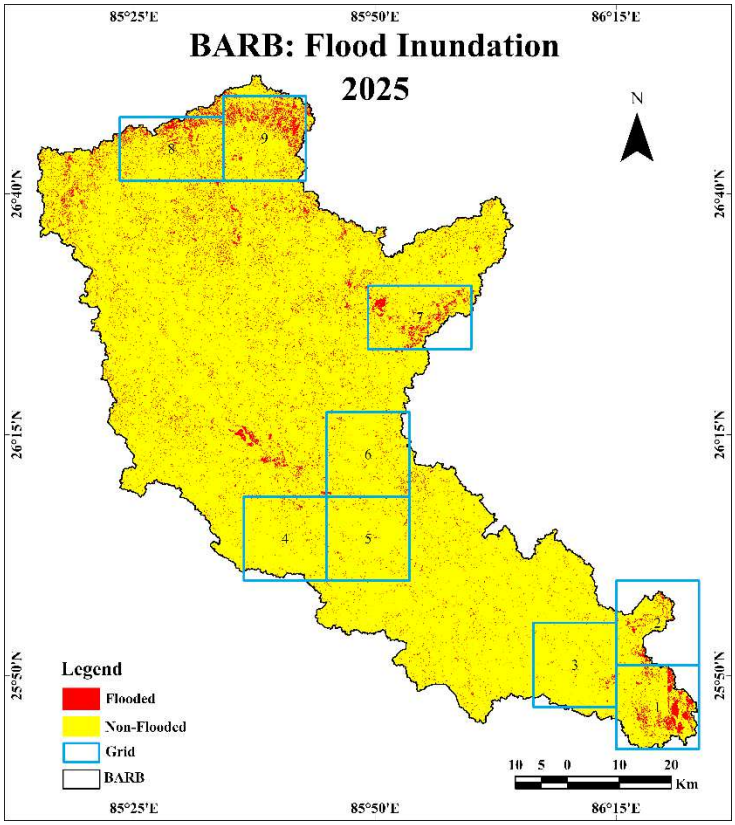

Fig.11d

Grid 5 in the middle catchment continues to be a major flood hotspot with denser clusters of inundation, while Grid 1, 2 and Grid 3 in the southeast also show significant flooded areas. Furthermore, Grid 4 and 6 show distinct linear flooding patterns associated with river channels and embankment overflows. Most of the northern upper catchment areas (Grids 8 and 9) remain dry and unflooded. The result revealed low flood inundation throughout the region in 2023 (Fig.11c). Flooding is virtually non-existent in the majority of the central and northern regions, encompassing Grids 4, 5, 6, 7, and 9. The southernmost basin outflow in Grids 1 and 2 is nearly the only location where moderate inundation clusters continue to exist, with only minor, faint linear traces visible along primary channel lines in Grid 8. The 2025 map shows (Fig.11d) moderate overall flood extent with a clear spatial change in susceptibility in the direction of the upper basin. Grid 1 in the lower catchment continues to experience persistent flooding, while there is a notable surge in inundation across the upper catchment grids (Grids 8 and 9) compared

to all other regions. Additionally, Grid 7 in the east becomes a prominent new flood hotspot, whereas Grids 4, 5, and 6 in the middle region show far less flooding than in 2017 and 2020. Spatiotemporal analysis of floods across the river basin reveals critical dynamics in flood distribution, persistence, and severity throughout the region. Overall, the results showed that 2017 was the most severe flooded year followed by 2020, 2025, and 2023 as the mildest year. Grid-wise statistical analysis showed that downstream grids consistently experienced higher flood percentages comparative to other grids (Table.2), indicating hydrologically realistic flood accumulation in lower catchment areas. The Lower Catchment and Middle Catchment saw a significant concentration of floods in the years 2017 and 2020. Grid 1 reached a peak of 34.4% in 2020, while Grid 2 reached a peak of 36.9% in 2017. Similarly, Grid 5 at 31.6% and Grid 4 at 18.98% show that the Middle Catchment experienced its highest flood levels in 2020. The findings for 2023 and 2025 show a distinct upward spatial shift of flood risk from downstream areas to upstream areas. Flooding in the Upper Catchment increased significantly from zero in a number of grids in 2020 to peak levels in 2025, with Grid 7 reaching 14.28%, Grid 8 reaching 15.22%, and Grid 9 reaching 19.36%.

Table 2: Changes in Flooded Area (In Percentage)

Grid / Year	Lower Catchment			Middle Catchment			Upper Catchment		
	1	**2**	**3**	**4**	**5**	**6**	**7**	**8**	**9**
2017	31.07	36.9	6.22	5.09	21.64	14.22	1.14	0.5	0
2020	34.4	21.17	16.96	18.98	31.6	9.37	0.57	0	0
2023	12.42	15.47	5.33	6.51	6.92	4	3.42	8.62	5.85
2025	17.51	10.58	1.78	2.77	2.59	4	14.28	15.22	19.36

Overall, Grid 1 exhibited the highest average flood percentage, while Grid 4 showed the greatest temporal variability, suggesting sensitivity to extreme rainfall and river overflow conditions. The analysis also revealed that 2017 and 2020 was a major flood year across several grids, whereas 2023 and 2025 showed unusually low flooding in lower-catchment grids but relatively higher flooding in upper-catchment areas. This anomaly may be associated with differences in rainfall distribution, acquisition timing, or local hydrological conditions.

Temporal consistency analysis further demonstrated strong interannual variability in flood occurrence, which is characteristic of monsoon-dominated river basins. The coefficient of variation indicated that some grids exhibited highly unstable flood behaviour, implying episodic flooding and localised hydrological influences. Despite these variations, the overall spatial flood pattern remained consistent with expected downstream flood concentration, thereby supporting the reliability of the SAR-derived flood maps.

5.7 Accuracy Assessment of Flood Inundation Mapping

An indicative accuracy assessment was also carried out using internal consistency analysis and visual verification of flood masks against mapped inundated areas. To estimate the categorization performance, a confusion matrix approach was employed. The indicative assessment produced an overall accuracy of approximately 90%, with producer's accuracy of 72% in 2021, 68 % in 2022 and user's accuracies of 69% in 2021 and 73% in 2022, also exceeding acceptable thresholds for flood mapping studies.

Table 3: Accuracy Assessment of Flooded Area

Metric	2021	2022

Overall agreement	91%	94%
Flood detection / Producer's Accuracy	72%	68%
Flood User's Accuracy	69%	73%
F1-score	70%	70%
Intersection over Union (IoU)	54%	54%
Cohen's Kappa	0.62	0.64

780

781 The value of Kappa Score is greater than 0.6, IoU is greater than 50% and also F1 score
782 is 70% in both years, all of which surpass permissible limits for flood mapping studies.
783 The flood extraction methodology therefore appears scientifically reliable for regional
784 flood assessment and temporal flood analysis.

785 However, some uncertainty may still arise due to SAR-specific limitations such as
786 vegetation masking, shadow effects, threshold sensitivity, and differences between image
787 acquisition dates and actual flood peaks. Since independent field-based ground-truth data
788 were not available, the accuracy assessment is indicative rather than absolute.
789 Nevertheless, the combination of SAR preprocessing, unsupervised flood classification,
790 grid-based inundation analysis, and temporal consistency testing provides a robust
791 methodological framework suitable for scientific flood mapping and hydrological
792 interpretation.

793 **6. Discussion**

794 **6.1 Hydroclimatic Changes in Baghmati -Adhwara River Basin**

795 Pearson correlation analysis from 2002 to 2024 in the BARB (Fig. 12a) showed a
796 positive correlation among rainfall, Evapotranspiration (ET), and Latent Heat Flux (LE)

(r = 0.5), indicating that higher rainfall is associated with increased ET and LE. A negative correlation with PET (r = -0.5) suggests that lower rainfall is associated with higher PET. Fig. 12b illustrates ET elasticity: a 1% increase in precipitation raises ET by 0.8%, whereas a 1% increase in PET decreases ET by 3.4%. Rainfall correlates positively with ET (Fig. 12c), but factors such as temperature, land cover, and soil moisture also influence ET. Lag correlation analysis (Fig. 12d) revealed weak or no time-shifted relationship, indicating that ET is mainly driven by same-year water availability.

A multi-line graph (Fig. 12e) shows that rainfall, ET, and PET vary over time. ET rises with rainfall, but PET decreases. Rainfall is highly variable and shows a declining trend, especially after 2020, leading to a rise in PET. To assess the basin's annual moisture status, an annual precipitation-to-PET ratio (AI = P/PET) was calculated (Fig. 12f). Here, (P) represents annual precipitation and (PET) represents annual potential evapotranspiration. Higher AI values indicate relatively humid or water-surplus conditions, while lower values indicate comparatively drier conditions and greater atmospheric water demand. Throughout the study period, annual precipitation generally exceeds PET, resulting in AI values greater than 1 and indicating an overall humid/water-surplus condition at the annual scale (Fig. 12f).

However, the annual water surplus does not necessarily imply continuous water availability. Most precipitation in the Baghmati-Adhwara River Basin occurs during the 3-4 monsoon months, producing substantial seasonal concentration of water input. Outside the monsoon season, reduced rainfall combined with persistent evaporative demand can cause soil-moisture depletion and reduced actual evapotranspiration. Furthermore, rapid runoff during intense rainfall events and limited soil-water storage can restrict the proportion of annual precipitation that remains available for evapotranspiration. The annual water deficit/surplus indicator (Fig. 12g) shows a

declining tendency, from approximately 4500 mm in the early part of the record to about 3500 mm by 2024, suggesting a gradual reduction in the magnitude of annual water surplus. The Standardized Water Deficit (Fig. 12h) further demonstrates substantial interannual hydro-climatic variability, including pronounced transitions between wet and dry conditions.

Since 2002, several years have experienced below-average water availability, with the recent period showing a tendency towards more persistent dry conditions. Since 2002, there have been 13 years of drier-than-average conditions, with recent years (since 2021) showing four consecutive dry years. Overall, BARB appears hydrologically contradictory: despite annual humidity, water stress persists due to rainfall variability, poor storage, and seasonal mismatches. A slight drying trend suggests increasing future water stress even with the current water surplus.

6.2 Hydro-Climatic Extremes: Spatiotemporal Dynamics and Cascading Impacts

According to the IPCC, human-induced climate change is impacting weather and climate extremes across the globe. Environmental conditions are becoming more fragile because of shifting rainfall patterns, rising global temperatures, and more severe and frequent hydrological extremes. Climate change is intensifying the global hydrological cycle, which alters the frequency and magnitude of extreme water events. It is also reshaping the spatial and temporal distribution of water-related hazards. Floods and droughts are among the most catastrophic natural hazards affecting human communities, economies, and ecosystems. These intense occurrences have an influence on water resources, particularly potable water for humans and sufficient water supply for agricultural activities. Urban and suburban communities are greatly affected by these extreme events

due to major land-use changes, rapid urbanisation and inefficient water management infrastructure.

Bihar, an eastern state of India, suffers from substantial multidimensional socioeconomic disadvantages like poverty, limited access to essential services, livelihood insecurity, and inadequate infrastructure, which make its communities more susceptible to climatic hazards. Baghmati- Adhwara River Basin, located in the Himalayan foothills, is more prone to hydrometeorological extremes and confronts the combined challenges of floods and droughts, characterised by rapid runoff from the steep catchment of the Himalayan rivers; high-intensity monsoons trigger devastating overbank flooding, while erratic monsoon or non-monsoon months bring prolonged droughts. Climate variability has further compressed rainfall into unpredictable patterns, exacerbating both acute flood periods and extended moisture deficits across the region.

These ongoing hydroclimatic extremes are affecting agriculture, physical infrastructure, natural ecosystems, and local socio-economic structures in the region. As an agrarian economy, this region is dependent on agriculture and allied activities for its livelihood and economic stability. Recurrent floods and droughts significantly reduce agricultural production by damaging standing crops and eroding fertile soil during crop-growth stages. Despite this, scarce rainfall and prolonged dry periods increase irrigation needs, reduce crop yields, and increase reliance on groundwater. Floods damage rural roads, bridges, and embankments, while heavy siltation raises riverbed levels and heightens future breach risks. Prolonged waterlogging in low-lying depressions destabilizes aquatic habitats and soil health, whereas dry spells severely deplete groundwater levels. These contrasting hydrometeorological disasters impact the economic activities of the dependent communities, making their condition miserable. Recurrent disasters in the

region pose significant challenges to sustainable industrial and economic development. Flooding disrupts industrial operations, damages assets, and limits access to industrial sites, whereas droughts reduce water availability for industry, agriculture, and other water-dependent economic activities. Heavy manufacturing and large-scale industrial investment are still lacking in this region due to disaster vulnerability. The constant threat of inundation fails to attract industrial development, leaving the region with no heavy enterprises that could generate stable non-agricultural employment. Consequently, agrarian communities suffer more and a lack of local industrial jobs forces widespread out-migration to distant urban centres in search of employment opportunities. Agro-based industries can be a major amplifier for economic prosperity in this region. This will bring opportunities for the locals, as it will provide a stable market for the producers, enhancing the agricultural income of the farmers along with employment opportunities for the people.

The lack of comprehensive, region-specific government policies, alongside severe implementation gaps in existing programs, makes the people of this region more vulnerable to the impact of disaster. While national frameworks like the National Disaster Management Authority (NDMA) guidelines and the Jal Jeevan Hariyali Mission exist on paper, their benefits are rarely found at the ground level where rural communities need them most. Top-down planning often fails to address the unique micro-realities of the region. Inadequate funding allocation and weak monitoring mechanisms keep flood relief, drainage restoration, and drought-mitigation initiatives largely ineffective, leaving vulnerable populations to face recurring disasters on their own. The region needs to connect local grassroots resilience with responsive national strategies.

7. Conclusion

The study analyzed spatial pattern of floods (2017-2025), long-term trends in rainfall variability and drought conditions in the Baghmati–Adhwara River Basin (BARB) from 1901 to 2024, utilizing the Sentinel-1 SAR data, Modified Mann-Kendall (MMK) test, the Standardized Precipitation Index (SPI), the Rainfall Anomaly Index (RAI), and rainfall forecasts based on XGBoost. The analysis reveals that 2017 and 2020 were major flood years across several grids, whereas 2023 and 2025 showed unusually low flooding in lower-catchment grids but relatively higher flooding in upper-catchment areas. While high interannual variability and localized hydrological drivers created temporal instability in flood occurrence, spatial analysis confirmed a consistent trend of downstream flood accumulation. Results also show a significant decline in annual rainfall across five of the six districts, with Madhubani (Sen's slope = -2.58 mm/year) and Darbhanga (-2.42 mm/year) experiencing the steepest decreases, followed by Samastipur, Sitamarhi, and Muzaffarpur. Sheohar shows a decline (-1.19 mm/year), but it is statistically insignificant.

Seasonal analysis shows that the monsoon season has the most widespread declining trend, with significant drops in Sitamarhi, Madhubani, Muzaffarpur, Darbhanga, and Samastipur. Winter rainfall also declines predominantly, with significant drops in Sitamarhi and Samastipur. Post-monsoon rainfall declines significantly in Sheohar and Madhubani, while Samastipur shows an increasing trend. Summer rainfall displays mixed patterns, declining in some northern regions and increasing in parts of the southern basin, although most changes are statistically insignificant. These seasonal shifts have key implications for agriculture. Less monsoon rainfall could increase water stress and irrigation needs during dry spells. Reduced post-monsoon and winter rainfall may lower residual soil moisture, raising irrigation demands for crops such as wheat,

pulses, oilseeds, vegetables, and horticultural produce. Variability in summer and pre-monsoon rainfall could also influence land preparation, crop planting, and early-season irrigation planning.

The SPI analysis reveals recurring precipitation deficits and wet conditions across multiple accumulation periods. SPI-3, SPI-6 and SPI-9 demonstrate short- to medium-term fluctuations in precipitation availability, whereas the SPI-12 series reveals prolonged annual-scale dry and wet episodes. The frequency of negative SPI-12 values has increased in several districts in recent decades, particularly after 2000, although occasional strongly wet years also occur. Thus, the SPI results indicate increased recurrence and persistence of long-term precipitation deficits rather than a uniform or uninterrupted drought across the basin. RAI results support this, showing more frequent negative rainfall anomalies, especially after 2000. The ET-PET relationship suggests periods of moisture stress despite the basin's substantial annual rainfall.

XGBoost projections through 2044 anticipate ongoing interannual rainfall variability in the BARB, with some districts, notably Darbhanga and Madhubani, likely experiencing lower rainfall. Together with observed decreases in annual and seasonal rainfall, especially during the monsoon, these forecasts imply growing uncertainties regarding water availability and timing for agriculture. The results show the region is facing floods and drought simultaneously, which is negatively affecting water resources, agricultural production, and livelihoods. Because paddy cultivation relies heavily on monsoon rains, reduced post-monsoon and winter moisture may ease irrigation needs for other crops, increasing dependence on groundwater and seasonal water stress. The region faces concurrent flood-drought, requiring channelization of flood flows for storage in chaurs and abandoned channels, which can be used during water deficit periods. To strengthen climate resilience, tailored measures such as rainwater harvesting, soil moisture

conservation during monsoon, efficient irrigation practices, drought-tolerant crops, and adjustments in sowing schedules and crop types are essential to adapt to shifting rainfall patterns.

However, the study is limited by the different spatial and temporal scales of the data used. Indices based on Rainfall data have been calculated from 1901 to 2024, while data of ET and PET were used from 2002 to 2023. Sentinel-1 SAR data has been used for flood inundation, which is available for very short time scales from 2017 to 2025.

Acknowledgments:

The authors acknowledge the Remote Sensing Lab, Advanced Research Centre Lab at L. N. Mithila University, Darbhanga, India, and the India Meteorological Department, Patna.

Contributions:

Study design and conceptualization: Manu Raj Sharma. Data collection: Manu Raj Sharma and Surbhi Kumari. Analysis and interpretation of results: Manu Raj Sharma and Surbhi Kumari. Writing – Original Draft: Manu Raj Sharma and Surbhi Kumari. 1st author and 2nd author reviewed and approved the final version of the manuscript.

Declarations

Ethics statement: Not applicable.

Data Availability: All data generated or analysed during this study are included in this published article.

Consent to participate: Not applicable, as this study did not involve human participants.

Consent to publish: Not applicable, as this manuscript does not contain any individual person's identifiable data.

Funding:

The authors received no funds or financial assistance for this work.

8. References

1. Clarke BJ, E. L. Otto F, Jones RG. Inventories of extreme weather events and impacts: Implications for loss and damage from and adaptation to climate extremes. Clim Risk Manag. Elsevier B.V.; 2021;32. https://doi.org/10.1016/j.crm.2021.100285

2. Borah G. Urban Water Stress: Climate Change Implications for Water Supply in Cities. Water Conservation Science and Engineering. Springer Nature; 2025. https://doi.org/10.1007/s41101-025-00344-5

3. Nations U, of Economic D, Affairs S, Division P. World Urbanization Prospects The 2018 Revision. 2018.

4. Güneralp B, Güneralp I, Liu Y. Changing global patterns of urban exposure to flood and drought hazards. Global Environmental Change. Elsevier Ltd; 2015; 31:217–25. https://doi.org/10.1016/j.gloenvcha.2015.01.002

5. Mustofa R, Sen MK, Hossain NUI, Zio E. A framework for the assessment of dynamic urban climate resilience considering effective water management system. Reliab Eng Syst Saf. Elsevier Ltd; 2027;277. https://doi.org/10.1016/j.ress.2026.113074

6. Adil Lina, Eckstein David, Kunzel Vera, Schafer Laura. Climate Risk Index 2026. 2025 Nov.

7. Trenberth KE, Fasullo JT, Shepherd TG. Attribution of climate extreme events. Nat. Clim. Chang. Nature Publishing Group; 2015. p. 725–30. https://doi.org/10.1038/nclimate2657

8. Westra S, Fowler HJ, Evans JP, Alexander L V., Berg P, Johnson F, et al. Future changes to the intensity and frequency of short-duration extreme rainfall. Reviews of Geophysics. Blackwell Publishing Ltd; 2014. p. 522–55. https://doi.org/10.1002/2014RG000464

9. Alfieri L, Dottori F, Betts R, Salamon P, Feyen L. Multi-model projections of river flood risk in Europe under global warming. Climate. MDPI AG; 2018;6. https://doi.org/10.3390/cli6010006

10. National Disaster Management Authority (NDMA). Annual Report 2020-21. New Delhi;

11. Singh R, Kumari M, Bindal S, Gupta I. Quantification of Drought Condition Using Drought Indices: A Review. In: Kolathayar S, Mondal A, Chian SC, editors. Climate Change and Water Security. Singapore: Springer Singapore; 2022. p. 231–41. https://doi.org/https://doi.org/10.1007/978-981-16-5501-2_19

12. Ministry of Agriculture and Farmers Welfare. Manual for Drought Management. New Delhi; 2020. https://doi.org/chrome-extension://efaidnbmnnnibpcajpcglclefindmkaj/https://vedas.sac.gov.in/static/pdf/Drought%20Manual-2020.pdf

13. OECD. Global Drought Outlook: Trends, Impacts and Policies to Adapt to a Drier World. Paris; 2025. https://doi.org/10.1787/d492583a-en.

14. World Meteorological Organization (WMO) and Global Water Partnership (GWP). Handbook of Drought Indicators and Indices (M. Svoboda and B.A. Fuchs). Integrated Drought Management Programme (IDMP), Integrated Drought Management Tools and Guidelines. Geneva; 2016. www.droughtmanagement.info

15. United Nations Office for Disaster Risk Reduction. Special Report on Drought 2021. Geneva; 2021. https://doi.org/https://www.undrr.org/publication/gar-special-report-drought-2021

16. Escriva-Bou A, Medellín-Azuara J, Hanak E, Abatzoglou J, Viers J. Drought and California's Agriculture. 2022 Apr. https://doi.org/https://www.ppic.org/wp-content/uploads/policy-brief-drought-and-californias-agriculture.pdf

17. United Nations Office for Disaster Risk Reduction. Global Assessment Report on Disaster Risk Reduction 2024: Forensic Insights for Future Resilience - Learning from Past Disasters. United Nations Publications; 2024. https://doi.org/https://www.undrr.org/gar

18. Toreti A, Bavera D, Navarro A, Acquafresca J, Azas L, Barbosa K, et al. Global Drought Overview September 2024 GDO Analytical Report. Luxembourg: Joint Research Centre (JRC), the European Commission's science and knowledge service.; 2024. https://doi.org/10.2760/7511271

19. Chandrasekara SSK, Kwon HH, Vithanage M, Obeysekera J, Kim TW. Drought in south asia: A review of drought assessment and prediction in south asian countries. Atmosphere (Basel). 2021;12. https://doi.org/10.3390/atmos12030369

20. Fiaz A, Rahman G, Kwon HH. Impacts of climate change on the South Asian monsoon: A comprehensive review of its variability and future projections. Journal of Hydro-Environment Research. Elsevier B.V.; 2025; 59:100654. https://doi.org/10.1016/j.jher.2025.100654

21. Liu Q, Huo A, Zhao Z, Zhao X, Rebouh NY, Luo C. Spatial Differentiation and Influencing Factors Analysis of Drought Characteristics Based on the Standardized Precipitation Index: A Case Study of the Yellow River Basin. Water (Switzerland). 2024;16. https://doi.org/10.3390/w16101337

22. Salimi H, Asadi E, Darbandi S. Meteorological and hydrological drought monitoring using several drought indices. Appl Water Sci. Springer Science and Business Media Deutschland GmbH; 2021;11. https://doi.org/10.1007/s13201-020-01345-6

23. Mujumdar M, Bhaskar P, Singh BB, Mangesh G, Ganeshi G. Severe Droughts in India. 1st ed. New York: Taylor & Francis Group; 2024. p. 191–206. https://doi.org/10.1201/9781003276555

24. Han J, Singh VP. Impacts of Drought in India and Preparedness for Drought Under Global Warming BT - Water Resources Management and Sustainability: Solutions for Arid Regions. In: Sefelnasr A, Sherif M, Singh VP, editors. Cham: Springer Nature Switzerland; 2025. p. 149–70. https://doi.org/10.1007/978-3-031-80520-2_9

25. Bharambe KP, Shimizu Y, Kantoush SA, Sumi T, Saber M. Impacts of climate change on drought and its consequences on the agricultural crop under worst-case scenario over the Godavari River Basin, India. Clim Serv. Elsevier B.V.; 2023; 32:100415. https://doi.org/10.1016/j.cliser.2023.100415

26. Choudhury A, Dutta D, Bera D, Kundu A. Regional variation of drought parameters and long-term trends over India using standardized precipitation evapotranspiration index. J Environ Manage. Elsevier Ltd; 2021; 296:113056. https://doi.org/10.1016/j.jenvman.2021.113056

27. Mckee TB, Doesken NJ, Kleist J. The Relationship of Drought Frequency and Duration to Time Scales. Eighth Conference on Applied Climatology. 1993.

28. Sharma MR, Priya S, Kumari S. Century of Rainfall Dynamics and Drought in Bihar: Patterns, Trends, and Climatic Variability (1901-2021). Current World Environment. 2025; 20:105–20. https://doi.org/10.12944/cwe.20.1.9

29. Asoka A, Gleeson T, Wada Y, Mishra V. Relative contribution of monsoon precipitation and pumping to changes in groundwater storage in India. Nat Geosci. Nature Publishing Group; 2017; 10:109–17. https://doi.org/10.1038/ngeo2869

30. Edwards DC. Characteristics of 20th Century Drought in the United States at Multiple Time Scales. [Fort Collins, Colorado]: Colorado State University; 1997.

31. Hayes M, Svoboda M, Wall N, Widhalm M. The Lincoln Declaration on Drought Indices: Universal Meteorological Drought Index Recommended. Bull Am Meteorol Soc. 2011;92:485–8. https://doi.org/10.1175/2010BAMS3103.1

32. Pandey AC, Kaushik K, Parida BR. Google Earth Engine for Large-Scale Flood Mapping Using SAR Data and Impact Assessment on Agriculture and Population of Ganga-Brahmaputra Basin. Sustainability (Switzerland). MDPI; 2022;14. https://doi.org/10.3390/su14074210

33. Rajput P, Verma MK, Ghodichore N, Sinha MK. Investigation of Spatiotemporal Changes of Drought Trend in Indian River Basin system over the century. Theor Appl Climatol. 2025;1 56:100. https://doi.org/10.1007/s00704-024-05328-4

34. Kaushik K, Pandey AC, Dwivedi CS. Microwave and optical satellite data fusion for meteorological drought monitoring in the Ganga-Brahmaputra basin. Theor Appl Climatol. Springer Vienna; 2024; 155:8989–9006. https://doi.org/10.1007/s00704-024-05177-1

35. Singh S, Jain V, Goyal MK. Evaluating climate shifts and drought regions in the central Indian river basins. Sci Rep. 2025; 15:1–21. https://doi.org/10.1038/s41598-025-15231-1

36. Dwivedi M, Mishra AK, Pandey RP, Suryavanshi S, Kumre SK. Evaluation of Drought in the Ken River Basin in Bundelkhand Region, India. International Journal of Environment and Climate Change. 2024; 14:419–36. https://doi.org/10.9734/ijecc/2024/v14i34053

37. Singh I, Mishra AK, Suryavanshi S, Sherring A, Kumar M. A Comparison of the Frequency and Intensity of Standardized Precipitation Index (SPI) and the Rainfall Anomaly Index (RAI) during the Meteorological Drought across Harohar-Punpun Basin (India). International Journal of Environment and Climate Change. 2024; 14:36–47. https://doi.org/10.9734/ijecc/2024/v14i64209

38. Singh U, Agarwal P, Sharma PK. Meteorological drought analysis with different indices for the Betwa River basin, India. Theor Appl Climatol. Springer; 2022; 148:1741–54. https://doi.org/10.1007/s00704-022-04027-2

39. Allen RG, Pereira LS, Raes D, Smith Martin. Crop Evapotranspiration Guidelines for computing crop water requirements-FAO Irrigation and drainage paper 56. FAO; 1998. https://doi.org/https://www.researchgate.net/publication/235704197_Crop_evapotranspiration-Guidelines_for_computing_crop_water_requirements-FAO_Irrigation_and_drainage_paper_56

40. Anderson MC, Norman JM, Mecikalski JR, Otkin JA, Kustas WP. A climatological study of evapotranspiration and moisture stress across the continental United States based on thermal remote sensing: 1. Model formulation. Journal of Geophysical Research Atmospheres. Blackwell Publishing Ltd; 2007;112. https://doi.org/10.1029/2006JD007506

41. Anderson MC, Hain C, Wardlow B, Pimstein A, Mecikalski JR, Kustas WP. Evaluation of drought indices based on Thermal remote sensing of evapotranspiration over the continental United States. J Clim. 2011;24:2025–44. https://doi.org/10.1175/2010JCLI3812.1

42. Vicente-Serrano SM, Beguería S, López-Moreno JI. A multiscalar drought index sensitive to global warming: The standardized precipitation evapotranspiration index. J Clim. 2010;23:1696–718. https://doi.org/10.1175/2009JCLI2909.1

43. Tripathi G, Chandra Pandey A, Ranjan Parida B. Rapid monitoring of peak monsoon flood during July-August 2020 over North Bihar plains using SAR data via Google Earth Engine platform.

44. Kumar A, Thangavel M. Unravelling the dynamics of rainfall patterns in Bihar, India: A comprehensive spatiotemporal analysis. Environmental Science and Pollution Research. Springer Berlin Heidelberg; 2025;32:8564–84. https://doi.org/10.1007/s11356-025-36243-4

45. Choudhary AK, Singh V. Drought Analysis Using Standardized Precipitation Index and Supplemental Irrigation Planning in Banka, Bihar BT - Hydrological Modeling: Hydraulics, Water Resources and Coastal Engineering. In: Jha R, Singh VP, Singh V, Roy LB, Thendiyath R, editors. Cham: Springer International Publishing; 2022. p. 125–38. https://doi.org/10.1007/978-3-030-81358-1_11

46. Srivastava H. Multi-temporal satellite imagery-based estimation of flood extent and population exposure in Central Bihar India. Discover Geoscience. Springer Nature; 2025;3. https://doi.org/10.1007/s44288-025-00210-w

47. Bhatt B, Shukla S, Bansal JK. Assessing Flood Risk and Emergency Preparedness in Gandak River Basin, Bihar, India using AHP. ISPRS Annals of the Photogrammetry, Remote Sensing and Spatial Information Sciences. Copernicus Publications; 2025. p. 51–8. https://doi.org/10.5194/isprs-annals-X-5-W2-2025-51-2025

48. Joyce KE, Belliss SE, Samsonov S V., McNeill SJ, Glassey PJ. A review of the status of satellite remote sensing and image processing techniques for mapping natural hazards and disasters. Prog. Phys. Geogr. SAGE Publications Ltd; 2009. p. 183–207. https://doi.org/10.1177/0309133309339563

49. Parida BR, Tripathi G, Pandey Arvind Chandra, Kumar A. Estimating floodwater depth using SAR-derived flood inundation maps and geomorphic model in Kosi River Basin (India). Geocarto Int. 2021; 15:4336–60. https://doi.org/https://doi.org/10.1080/10106049.2021.1899298

50. Khan KM, Wang B, Dey H, Pradhananga D, Smith LC. Flood Susceptibility Mapping of the Kosi Megafan Using Ensemble Machine Learning and SAR Data. Remote Sens (Basel). Multidisciplinary Digital Publishing Institute (MDPI); 2026;18. https://doi.org/10.3390/rs18081158

51. Tuladhar D, Dewan A, Kuhn M, Corner RJ. Spatio-temporal rainfall variability in the Himalayan mountain catchment of the Bagmati River in Nepal. Theor Appl Climatol. Theoretical and Applied Climatology; 2019;139:599–614. https://doi.org/10.1007/s00704-019-02985-8

52. Kumari S, Sharma MR. Analysis of Rainfall Trends and Drought over the Bagmati-Adhwara River Basin (1901-2022). Geographical Perspective. 2025;26:335–45. https://doi.org/https://www.researchgate.net/publication/397411685_analysis_of_rainfall_trends_and_drought_over_baghmati-adhwara_river_basin_1901-2022?_tp=eyJjb250ZXh0Ijp7ImZpcnN0UGFnZSI6ImhvbWUiLCJwYWdlIjoic2VhcmNoIiwicG9zaXRpb24iOiJwYWdlSGVhZGVyIn19

53. Chandran R. Vinu, Ramakrishnan D, Chowdary V M, Jeyaram A, Jha A M. Flood mapping and analysis using air-borne synthetic aperture radar: A case study of July 2004 flood in Baghmati river basin, Bihar. Curr Sci. 2006;90. https://doi.org/https://www.researchgate.net/publication/257923296_Flood_mapping_and_analysis_using_airborne_synthetic_aperture_radar_A_case_study_of_July_2004_flood_in_Baghmati_river_basin_Bihar

54. Sharma MR, Das SK, Shankar A, Chandel VBS. Climate Change and Sustainable Adaptation: An Analysis of the Effects of Rainfall Variability on Wetland Ecosystems in Madhubani, Bihar, India. Sustainable Development Goals Series. Springer; 2026. p. 33–50. https://doi.org/10.1007/978-3-031-96977-5_3

55. Sharma MR, Das SK. Integrated eco-hydrological and vegetation productivity analysis of wetland landscapes in Madhubani, Bihar (2002–2024). Sci Rep. Springer Science and Business Media LLC; 2026; https://doi.org/10.1038/s41598-026-60072-1

56. Kumar P, Deka D, Yadav A, Ashwani, Kumar M, Das JP, et al. Potential and actual evapotranspiration and Landsat-derived indices. Global Journal of Environmental Science and Management. 2024; 10:1227–48. https://doi.org/10.22034/gjesm.2024.03.18

57. Union E. Standardized Precipitation Index (SPI): EDO and GDO Indicator Factsheet. US Weather Bureau, Res Pap No 45. 2025;58. https://doi.org/https://www.ncdc.noaa.gov/temp-and-precip/drought/docs/palmer.pdf

58. Aryal A, Maharjan M, Talchabhadel R, Thapa BR. Characterizing Meteorological Droughts in Nepal: A Comparative Analysis of Standardized Precipitation Index and Rainfall Anomaly Index. Earth (Switzerland). 2022; 3:409–32. https://doi.org/10.3390/earth3010025

59. Tigkas D, Vangelis H, Tsakiris G. DrinC: a software for drought analysis based on drought indices. Earth Sci Inform. Springer Verlag; 2015;8:697–709. https://doi.org/10.1007/s12145-014-0178-y

60. van Rooy MP. A Rainfall Anomaly Index Independent of Time and Space. Notos. South African Weather Bureau; 1965; 14:43–8.

61. Anwar MT, Winarno E, Hadikurniawati W, Novita M. Rainfall prediction using Extreme Gradient Boosting. J Phys Conf Ser. 2021;1869. https://doi.org/10.1088/1742-6596/1869/1/012078